The Canadian Mineralogist
Vol. 44, pp. 229-248 (2006)

MANGANESE-RICH ASSEMBLAGES IN THE BARRHORN UNIT, TURTMANNTAL, CENTRAL ALPS, SWITZERLAND

JOËL BRUGGER§

School of Earth and Environmental Sciences, The University of Adelaide, North Terrace, 5005 Adelaide, South Australia, and Division of Mineralogy, South Australian Museum, North Terrace, 5000 Adelaide, South Australia, Australia

NICOLAS MEISSER

Musée Cantonal de Géologie et Laboratoire des Rayons X, Institut de Minéralogie et de Géochimie, UNIL-BFSH2, CH-1015 Lausanne-Dorigny, Switzerland

ABSTRACT

The Triassic carbonates of the Briançonnais Domain in Turtmanntal, Western Swiss Alps, contain lenses up to 3 m across filled with Mn- and Fe-rich sediments. These rocks display a fine compositional banding at a millimetric scale, and consist of alternating carbonate layers (kutnohorite, dolomite, rhodochrosite and calcite), oxide layers (jacobsite; reduced horizons with manganosite ± hausmannite; Fe-rich zones with magnetite and hematite) and silicate layers (spessartine, manganocummingtonite, ± tephroite, fluorapatite). Minerals of vanadium, including pyrobelonite, turtmannite, reppiaite and sarkinite, occur in the main schistosity and in discordant veinlets. Other accessory minerals include crednerite, pennantite, barite, pyrite, chalcopyrite, bornite(?), native copper and algodonite. Quaternary weathering resulted in the formation of birnessite, takanelite, nsutite–ramsdellite, hollandite, manganite, pyrolusite, cuprite and malachite. The Pipji Mn-rich sediments were originally interpreted as residual sediments deposited in karstic cavities during Middle Jurassic. However, a hydrothermal input is indicated by the low REE contents and MREE enrichment of the hydrothermal end-member composition relative to PAAS, a large range in V:As ratios, and low U and Th contents. Low silica contents suggest a low-temperature hydrothermal fluid (≤60°C). The Pipji occurrence hence is related to Mesozoic exhalative Mn-rich sediments from the Briançonnais, Helvetic and Piemont domains of the Alps. Comparison of the Pipji Mn-rich rocks with Alpine occurrences of exhalative, residual and hydrogenous origins shows that discrimination diagrams based upon transition metals are useful for interpreting the petrology of Mn-rich rocks within particular depositional environments, but cannot be generalized to different settings. The Pipji Mn-rich lenses developed their present mineralogy during Tertiary metamorphism under upper greenschist-facies conditions. They are characterized by relatively reduced parageneses, including the manganosite–jacobsite association. This association is stable under conditions for which CO_2 and CH_4 coexist in the gas phase, suggesting that the redox state of the Mn-rich mineral assemblage during metamorphism was buffered by the graphite-bearing dolomitic marble hosting the lenses.

Keywords: metamorphism, manganese deposit, geochemistry, rare-earth elements, synsedimentary exhalative deposit, Swiss Alps.

SOMMAIRE

Les carbonates triassiques du domaine Briançonnais dans le Val Tourtemagne (Alpes Suisses) contiennent des lentilles métriques remplies de sédiments riches en Mn et Fe. Ces roches sont finement litées (mm), avec des niveaux à carbonates (kutnohorite, dolomite, rhodochrosite et calcite), oxydes (jacobsite; niveaux réduits à manganosite ± hausmannite; niveaux ferrugineux à magnétite et hématite) et silicates (spessartine, manganocummingtonite, ± téphroïte, fluorapatite). Des vanadates (pyrobélonite, turtmannite, reppiaïte et sarkinite vanadifère) sont présents dans la schistosité principale et dans des veinules discordantes. Parmi les autres minéraux accessoires, on trouve crednérite, pennantite, barite, pyrite, chalcopyrite, bornite(?), cuivre natif et algodonite. Birnessite, takanélite, nsutite–ramsdellite, hollandite, manganite, pyrolusite, cuprite et malachite se sont formées durant l'altération quaternaire. Les sédiments manganésifères de Pipji ont été interprétés originellement en tant que sédiments résiduels déposés dans des cavités karstiques durant le Jurassique moyen. Cependant, la géochimie indique la présence d'une composante hydrothermale caractérisée par de basses teneurs en terre rares, U et Th, un enrichissement en terres rare moyennes par rapport à PAAS, et un large éventail de rapports As:V. La basse teneur en silice suggère une basse température du fluide hydrothermal (≤60°C). Pipji est donc un nouvel exemple de sédiment exhalatif triassique. La comparaison de Pipji avec les exhalatites décrites

§ *E-mail address*: joel.brugger@adelaide.edu.au

dans les domaines Briançonnais, Helvétique et Piémontais ainsi qu'avec des sédiments résiduels et hydrogéniques Alpins démontre que les diagrammes discriminants fondés sur les métaux de transition sont utiles dans l'interprétation de la pétrologie des roches manganésifères dans un contexte génétique donné, mais ne peuvent être généralisés à d'autres environnements. La paragenèse minérale des lentilles manganésifères de Pipji s'est développée durant le métamorphisme Alpin sous faciès schiste vert supérieur. Elle est caractérisée par des associations relativement réduites à manganosite et jacobsite. Cette association est stable en présence d'une phase gazeuse contenant CO_2 et CH_4, suggérant que l'état d'oxydation des lentilles était contrôlé par les dolomites graphitiques dans lesquelles elles sont encaissées.

Mots-clés: métamorphisme, gisement de manganèse, géochimie, terres rares, gisement synsédimentaire exhalatif, Alpes Suisses.

Introduction

The Mesozoic rocks of the Alpine Arc contain a number of syngenetic exhalative Mn–Fe deposits hosted in Triassic (*e.g.,* Val Ferrara, Central Alps; Brugger & Gieré 2000) and Jurassic (*e.g.*, Gonzen, Central Alps; Pfeifer *et al.* 1988) platform carbonates or in Jurassic sediments of the Piedmont Domain typical of abyssal plains [*e.g.*, Ködnitz Valley, Eastern Alps; Abrecht (1990); Graubünden, Central Alps; Geiger (1948); Praborna and Val Graveglia, Southern Alps; Martin-Vernizzi (1984), Cortesogno *et al.* (1979); Haute-Maurienne, Western Alps; Chopin (1978)]. These deposits are all related to the opening of the Tethys Ocean: the Triassic deposits document early rifting, and Jurassic deposits, the spreading stage of the ocean floor. The deposits underwent Alpine metamorphism under conditions ranging from very low grade (Gonzen, Val Graveglia) to eclogitic facies (Praborna). They developed complex assemblages of metamorphic minerals, as well as rich associations of minor phases containing trace elements such as As, V, Sb, the rare-earth elements (REE), and Be (*e.g.*, Geiger 1948, Abrecht 1990, Basso *et al.* 1992, Perseil & Smith 1995, Smith & Perseil 1997, Brugger & Gieré 1999, 2000), depending upon the geochemistry of the protolith, the conditions of metamorphism, and the nature and extent of retrograde hydrothermal remobilization (Brugger & Gieré 2000).

In this paper, we describe with geological, mineralogical, and geochemical data a new occurrence of Mn-rich rocks hosted in the Triassic carbonates of the Barrhorn Series (Briançonnais Domain) at Pipjitälli, Turtmanntal, Western Swiss Alps. The Mn-rich rocks have undergone regional upper-greenschist-facies metamorphism, and are remarkable for the presence of reduced horizons with manganosite and hausmannite, and for the relative abundance of a suite of V- and As-bearing minerals, including the recently described new mineral turtmannite (Brugger *et al.* 2001). We discuss the origin of the Mn-rich rocks and their unusual mineralogical assemblage, their relationships with other occurrences of Mn-rich rocks in the Alps and beyond, and the implications for the geological evolution of the Briançonnais domain.

Geological Setting

The Turtmanntal, a tributary to the Rhone Valley in Canton Wallis, Western Switzerland, belongs to the Middle Penninic (Briançonnais paleogeographic domain) Siviez–Mischabel super-nappe (Escher *et al.* 1987; Fig. 1). In the upper part of the valley, the pre-Mesozoic crystalline rocks of the "Ensemble de l'Ergischhorn" are overlain by the sediments of the Barrhorn Series. The Barrhorn Series is one of the rare Mesozoic covers of the Briançonnais domain that is still bound to its original basement (Sartori 1990). The Briançonnais domain acted as a high between the troughs of the Lower and Upper Penninic domains in the Jurassic. This inference is reflected by the sedimentary sequence of the Barrhorn Series (Fig. 2): Triassic (Ladinian and Carnian) dolomitic marbles are overlain by Middle Jurassic (Dogger) sediments comprising basal conglomerate, piemontite- and white-mica-bearing quartzite, black micaschist, calcareous quartzite, and black marble. The Middle Jurassic sediments are overlain by Upper Jurassic (Malm) platform carbonates (grey marble). The Mn-rich pockets are embedded in grey dolomitic marble of the Ladinian "Couches à Constatoria Goldfussi". Locally, the Middle Jurassic series is reduced to a metabauxite (*sensu lato*) horizon intercalated between the Triassic dolomitic marble and the Malm marble (*e.g.*, Baud *et al.* 1977, Poinssot *et al.* 1997). Similar aluminous sediments are found in paleokarst pockets within the Triassic marbles. Such continental deposits are common in the Briançonnais Domain, and can be traced from the Apuane Alps to Liguria to the Barrhorn Series. These deposits are usually Al-rich and locally Fe-rich (up to 31.4 wt% Fe_2O_3), but they contain little Mn (≤0.63 wt% MnO; Poinssot *et al.* 1997). They are enriched in trace elements such as F, Li, Be, HFSE and REE. According to Poinssot *et al.* (1997), this geochemical signature indicates that the residual sediments developed over a granitic basement and were transported into their current location, which precludes an *in situ* origin by weathering. A granite-rich hinterland, possibly the Corso-Sardinian basement, thus seems to have drained into the Briançonnais Domain during the Middle Jurassic. These results hence support

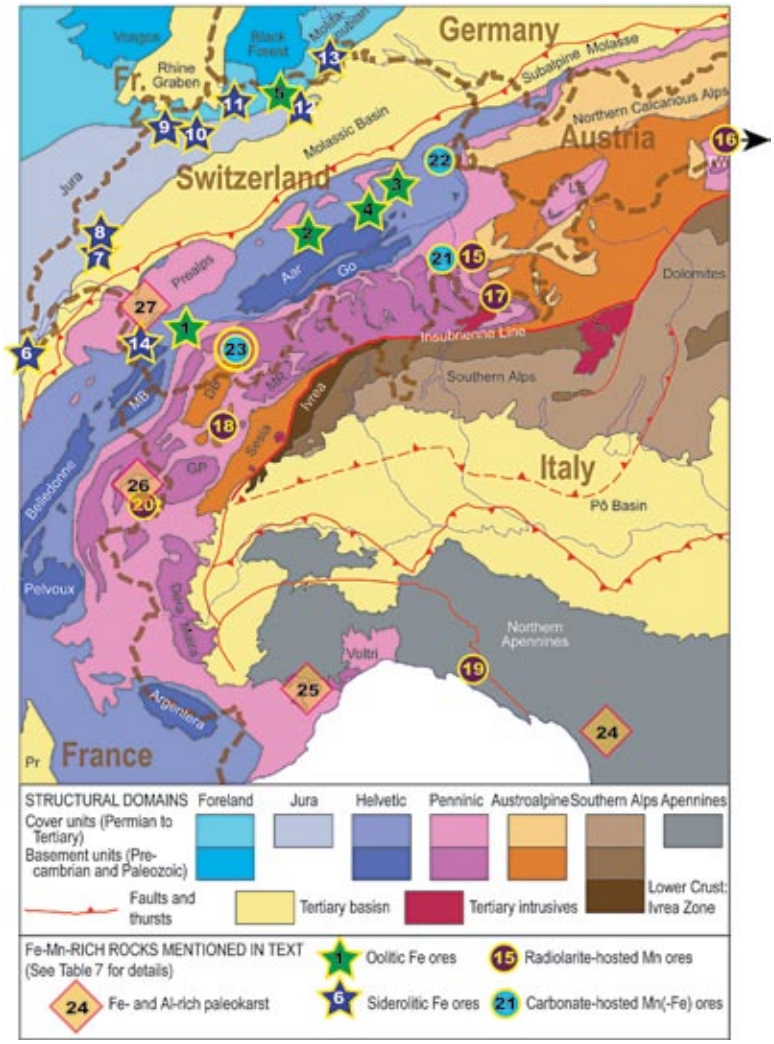

FIG. 1. Location of the occurrences of Fe- and Mn-rich rocks mentioned in this paper, with relation to the Alpine tectonics. Localities are listed in Table 7. Background map modified after Berthelsen *et al.* (1992).

an exotic origin for the Briançonnais (*e.g.*, Stampfli 1993). The Mn-rich rocks at Pipji have been interpreted to represent a Mn-rich variety of these residual sediments (Sartori 1990).

The Mn-rich sediments and the surrounding rocks were subjected to a Tertiary regional greenschist-facies metamorphism culminating at about 450°C at pressures of 4 to 6 kbar (Sartori 1990). During metamorphism, the Mn-rich rocks at Pipji developed a complex assemblage of minerals (Table 1), described in detail below. Note that some karst-filling meta-argillite and bedded siliceous metabauxite of the Barrhorn Series also evolved complex and unusual mineralogy during metamorphism: they are the type locality for zincostaurolite (Chopin *et al.* 2003) and also contain abundant cookeite, accessory florencite-(Ce) and chromian gahnite (Meisser *et al.* 2004).

OCCURRENCE OF Mn-RICH SEDIMENTS IN THE BARRHORN SERIES

Manganese-rich rocks were discovered by Sartori (1990) in the cliff forming the left rim of the ice fall of the Pipjigletscher in Turtmanntal, at coordinates

112.450/622.550 (Swiss National Reference System). The Mn-rich rocks occur as two flattened lenses, the largest one measuring 3 m by 0.4 m (Fig. 3a).

In situ observations of the lenses are limited owing to the dangerous location (cliffs with common rockfalls). Most observations rely on systematic sampling of abundant scree material directly underneath the lenses. The disposition and internal structure of the lenses were observed by S. Ansermet during a short visit in 2002 (Fig. 3a). The lenses appear massive; the contacts are highly deformed and seem compatible with a paleokarst setting, but do not exclude a syngenetic exhalative origin. Thin (mm to cm) layers rich in Mn oxides seem to exist in stratigraphic continuity with the Triassic carbonates (*e.g.*, Fig. 3c) and are in some cases folded together with the marble. These provide evidence for an early, syngenetic or diagenetic enrichment of manganese.

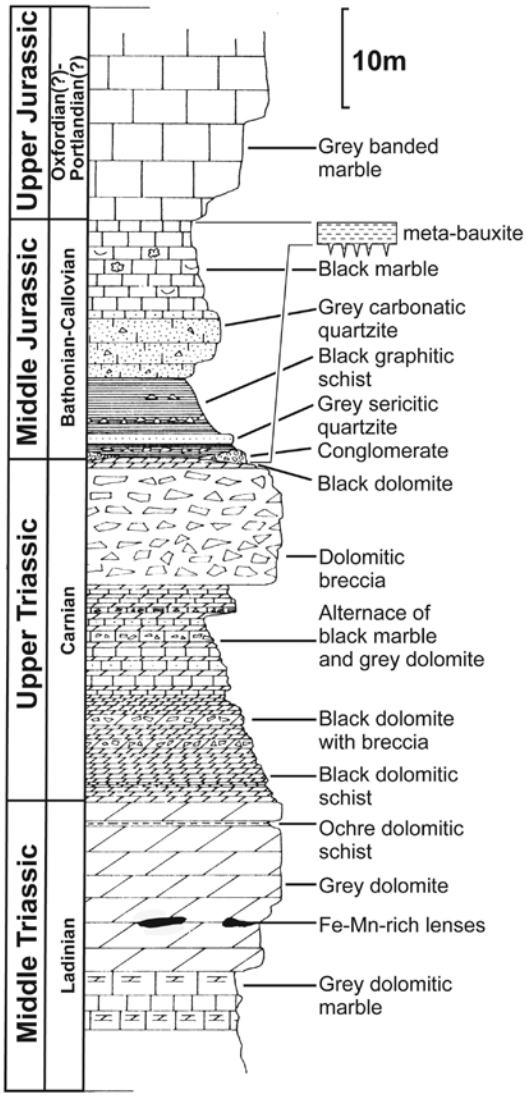

FIG. 2. Stratigraphic profile of Mesozoic formations at Pipji. At Bruneggjoch, about 3 km to the southeast, the Middle Jurassic is reduced to a metabauxite horizon. Modified after Sartori (1990).

The Mn-rich rocks usually display a fine (0.2–10 mm) compositional banding, consisting of an alternation of beds with different proportions of oxide, carbonate, and silicate minerals (Fig. 3b). The main minerals aligned in the main schistosity (S_1) are dolomite, kutnohorite, jacobsite, magnetite, and spessartine. Although the compositional zoning is most likely of premetamorphic origin, the minerals constituting it recrystallized during the Alpine metamorphism into an equigranular texture. Foliation S_1 is parallel to the bedding, S_0. Both S_0 and S_1 are deformed by small-scale (cm to dm) folds (Fig. 3b). Moreover, the Mn-rich rocks are cut by thin veinlets <1 cm wide containing mainly white to pink rhodochrosite. Locally, supergene alteration of probable Quaternary age resulted in the formation of black, porous crusts. A list of minerals identified from the Mn-rich rocks as well as the association from five thin sections are given in Table 1.

MINERALOGY OF THE MN-AND FE-RICH ROCKS

Methods

Polished thin sections from ten samples collected in the scree have been studied using reflection and transmission optical microscopy, quantitative electron-microprobe (EMP) analysis, scanning electron microscopy (SEM) connected to qualitative energy-dispersion spectrometry (EDS), and powder X-ray diffraction (XRD) using a diffractometer, and Gandolfi and Debye–Scherrer cameras.

Carbonate layers

Dolomite and kutnohorite are concentrated in fine-grained beds up to 1 mm in thickness, with minor jacobsite, magnetite and spessartine. It seems that in this association, dolomite (with a characteristic diffraction-peak at 2.85 Å) is less abundant than kutnohorite (characteristic peak at 2.94 Å). The kutnohorite, commonly associated with xenomorphic grains of strontian barite (2–3 wt% SrO), contains several wt% SrO. The replacement of jacobsite grains by kutnohorite also is observed locally. The kutnohorite from Pipjigletscher displays an excess in calcium, with an average formula $Ca_{1.16}Mn_{0.83}Mg_{0.10}Sr_{0.01}(CO_3)_2$ (average results of four analyses).

Oxide layers

Jacobsite forms xenomorphic aggregates up to 100 μm across, and contains minor amounts of Al (up to 4.50 wt% Al_2O_3), V (up to 0.42 wt% V_2O_3), Ti (up to 0.19 wt% TiO_2), Mg (up to 0.25 wt% MgO), Ni (up to 0.84 wt% NiO), Co (up to 0.13 wt% CoO) and Cu (up to 0.07 wt% Cu_2O) (Table 2). The jacobsite–carbonate beds also contain small amounts of bravoite as xenomorphic grains <100 μm in size, partially replaced by

TABLE 1. MINERALOGICAL ASSOCIATIONS IN THE MANGANIFEROUS LENSES AT PIPJIGLETSCHER

Phase 1: *Metamorphic minerals within the main schistosity*		*#2*	*#3*	*#5c*	*#6*	*#7*
Jacobsite (Jcb)	$(Mn^{2+},Fe^{2+},Ni)(Fe^{3+},Mn^{3+},V^{3+})_2O_4$	×	×	×	×	×
Magnetite (Mgt)	$Fe^{2+}Fe^{3+}{}_2O_4$				×	
Hausmannite (Hsm)	$Mn^{2+}Mn^{3+}{}_2O_4$		×	×		
Galaxite (Gal)	$(Mn^{2+},Mg)(Al,Fe^{3+})_2O_4$			×		
Manganosite (Mns)	MnO		×	×		×
Pyrophanite	$MnTiO_3$				×	
Kutnohorite (Kt)	$Ca(Mn,Mg,Sr)(CO_3)_2$	×	×			×
Rhodochrosite (Rds)	$MnCO_3$			×		×
Calcite (Cal)	$CaCO_3$		×			
Dolomite	$CaMg(CO_3)_2$					
Spessartine (Sps)	$Mn_3Al_2(SiO_4)_3$	×			×	
Tephroite (Tep)	$Mn^{2+}{}_2SiO_4$	×	×			
Manganocummingtonite	$Mn_2Mg_5Si_8O_{22}(OH)_2$				×	
Ribbeite (?) (Rib)	$(Mn,Mg)_5(SiO_4)_2(OH)_2$			×		
Biotite	$K(Mg,Fe)_3(Si_3Al)O_{10}(OH,F)_2$				×	
Talc-2*M*	$Mg_3Si_4O_{10}(OH)_2$					
Barite (Brt)	$(Ba,Sr)SO_4$ (2–3% SrO)	×		×	×	
Fluorapatite (Ap)	$Ca_5(PO_4)_3F$				×	
Pyrite	FeS_2			×		
Chalcopyrite	$CuFeS_2$				×	
Bornite (?)	Cu_5FeS_4					
Native copper	Cu	×			×	
Algodonite	Cu_6As	×				
Pyrobelonite (Prb)	$(Pb,Sr,Ba)(Mn,Ca)(VO_4)(OH)$	×	×	×	×	
Turtmannite (Trt)	$(V,As)_2As^{3+}Si_3(Mn,Mg)_{22.5}O_{48}H_{21}$	×				
Unknown#1 (U#1)	$(V,As)_2(Mn,Mg)_7O_{18}H_{12}$		×			
Unknown#2 (U#2)	$(V,As,Si)_4Si_2(Mn,Mg)_{24}O_{57}H_{38}$		×	×		
Unknown#3 (U#3)	$(V,As,Si)_4Si_2(Mn,Mg)_{22}O_{47}H_{22}$	×				
Reppiaite	$Mn_5[(V,As)O_4]_2(OH)_4$	×	×	×		
Sarkinite	$Mn_2[(As,V)O_4](OH)$					
Phase 2: *Metamorphic minerals in fractures discordant relative to S_1*						
Kutnohorite	$(Ca,Mn)(CO_3)_2$					×
Rhodochrosite (Rdc)	$MnCO_3$					×
Crednerite (Crd)	$CuMnO_2$					×
Manganite ± pyrolusite	$MnO(OH) \pm MnO_2$					
Pennantite	$Mn^{2+}{}_5Al(Si_3Al)O_{10}(OH)_8$				×	×
Titanite	$CaTiSiO_5$					×
Turtmannite (Trt)	$(V,As)_2As^{3+}Si_3(Mn,Mg)_{22.5}O_{48}H_{21}$	×				
Phase 3: *supergene alteration*						
Birnessite	$(Ca, Na, K)(Mg, Mn)Mn_6O_{14}•5H_2O$					×
Takanelite	$(Mn^{2+},Ca)_{0.2}Mn^{4+}O_2•0.7H_2O$		×			
Nsutite–ramsdellite	MnO_2-Hex or MnO_2-Orth					
Hollandite	$Ba(Mn^{4+},Mn^{2+})_8O_{16}$					
Manganite (Man)	$Mn^{3+}O(OH)$					×
Pyrolusite	MnO_2 (tetragonal)					×
Cuprite	Cu_2O	×			×	
Malachite	$Cu_2CO_3(OH)_2$					

cobaltite. The EMP analytical data give the following formula for the cobaltite: sample $(Co_{0.93}Ni_{0.06})As_{0.93}S_{1.08}$. Hematite-rich blocks (*e.g.*, sample Pigl.9) occur scarcely in the scree, and seem to originate from a yet-undiscovered pocket or lens. The hematite in Pigl.9 is associated with magnetite, kutnohorite and calcite.

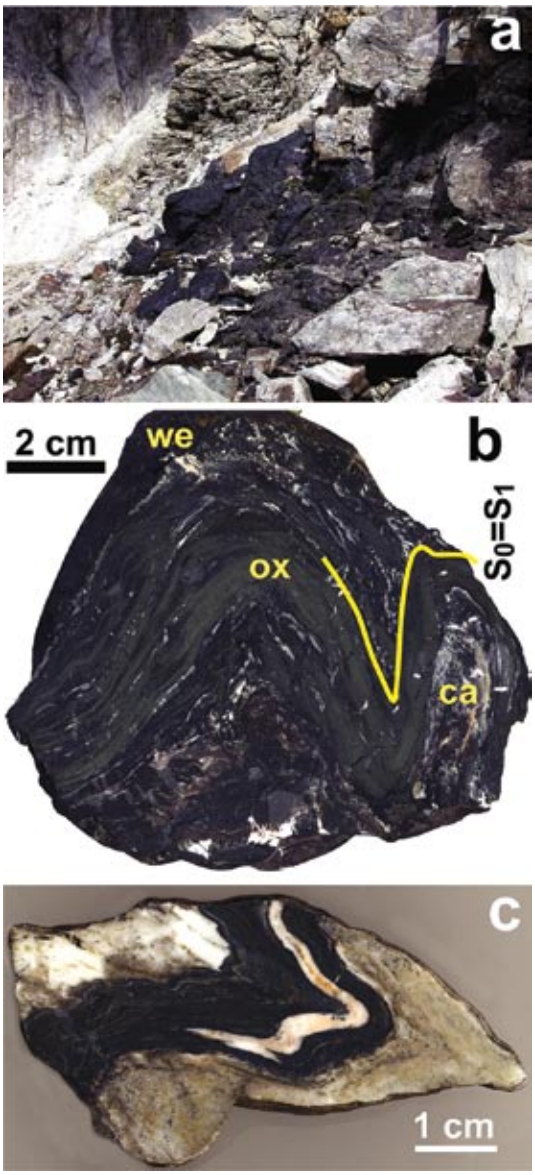

FIG. 3. Mn-rich rocks from Pipji, Turtmanntal, Switzerland. (a) The main pocket lies conformably in Triassic dolomitic marble. The length of the lens is about 3 m. Photo: Stefan Ansermet. (b) Layered oxide (ox; consisting mainly of greenish jacobsite) and carbonate (ca) facies. A deep black crust consisting of secondary Mn^{4+}-bearing minerals can be seen on the upper part of the sample (we). (c) Finely banded Mn-rich rock in apparent stratigraphic continuity with Triassic dolomitic marble.

The Mn^{2+} oxide manganosite was observed only in few samples (Pigl.3, Pigl.5, Pigl.7 in Table 1). EMP analyses of manganosite show small quantities of transition metals (*e.g.*, up to 0.30 wt% NiO, 0.22 wt% CoO; Table 2), as well as Mg, V and As (up to 0.83 wt% MgO, 0.78 wt% V_2O_3 and 0.95 wt% As_2O_3; Table 2). The unit-cell parameter *a* is 4.439(2) Å. Manganosite forms emerald-green beds, less than 1 mm in width, that also contain small inclusions of hausmannite, Mn_3O_4, dispersed grains of arsenian native copper (< 100 μm), and isolated xenomorphic grains of pyrobelonite and reppiaite (Figs. 4b, g, h). Hausmannite contains small amounts of Fe, Al, V and Ni (up to 2.39 wt% Fe_2O_3, 0.41 wt% Al_2O_3, 0.08 wt% V_2O_3, and 0.17 wt% NiO; Table 2). The unit-cell parameters of the chemically analyzed hausmannite are *a* 5.783(1), *c* 9.402(3) Å. Some grains of native arsenic-rich copper grains display a thin rim (<5 μm) of algodonite and cuprite. Sample Pigl.3 also contains small needles (up to 65 μm in length) of an unidentified vanadate (unknown #2; Fig. 4a). Sample Pigl.5 contains xenomorphic grains (up to 50 μm in size) of the spinel-group mineral galaxite, embedded in manganoan calcite and rhodochrosite (Fig. 5c). The average composition (Table 2) is $Galaxite_{0.60}Spinel_{0.31}Hausmannite_{0.07}Jacobsite_{0.02}$, where spinel stands for $Mg_{0.63}Ni_{0.27}Co_{0.05}Zn_{0.04}Al_2O_4$. The galaxite is associated to porphyroblastic manganoan calcite, interstitial rhodochrosite and a hydrated Mn-silicate, probably ribbeite (Table 3).

Magnetite, Fe_3O_4, occurs as small grains in silicate-rich beds or embedded in hematite lamellae. EMPA show that the magnetite associated with spessartine contains up to 2–4% MnO and 1–2% V_2O_5. In the asso-

FIG. 4. Microphotographs of the manganiferous rocks from Pipji. (a) Needles of the vanadate Unknown #2 embedded in hausmannite + jacobsite. Reflected light, slightly crossed polars. Pigl.3. (b) Pyrobelonite grains in hausmannite + kutnohorite ± manganosite. Reflected light, crossed polars, oil immersion. Pigl.3, photo: Elena-Adriana Perseil. (c) Carbonate-rich layer containing turtmannite and the vanadate Unknown #3. Pigl.2, transmitted light, parallel polars. (d) Close-up view of two crystals of turtmannite. The crystal on the right has been cut by a discordant vein, but did grow during the opening of the vein. Pigl.2, transmitted light, parallel polars. (e) Crednerite with manganite in a veinlet cross-cutting Pigl.7. Reflected light, crossed polars. (f) Spessartine (Sps) with pyrophanite. The numerous inclusions in spessartine are fluorapatite. Pigl.6, transmitted light, parallel polars. (g) Manganosite-rich layer containing pyrobelonite and the vanadate Unknown #1. Pigl.3, transmitted light, parallel polars. (h) Needle of the vanadate Unknown #2. Pigl.5, transmitted light, parallel polars. For abbreviations, see Table 1.

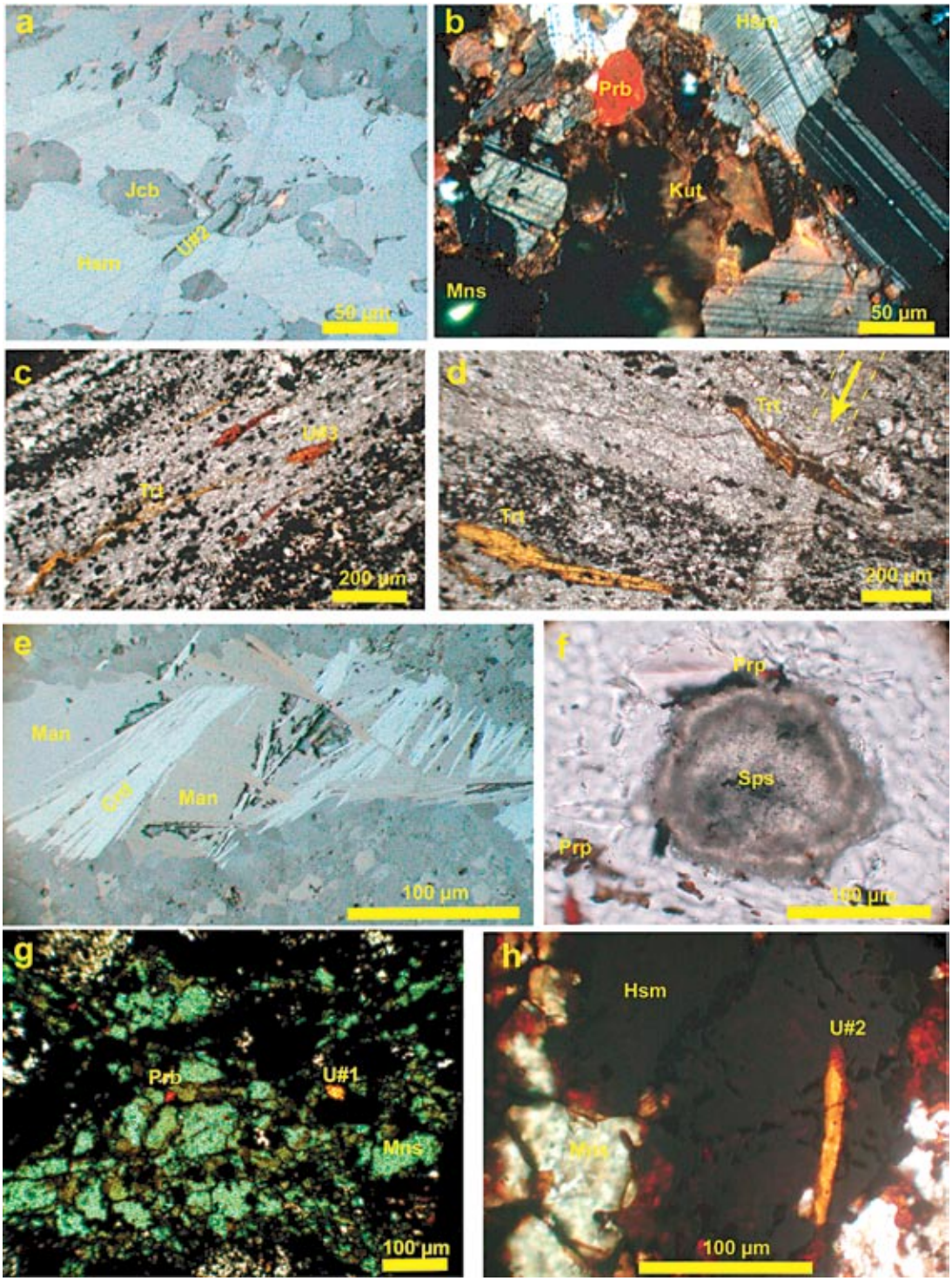
a
Jcb
U#2
Hsm
50 µm
b
Hsm
Prb
Kut
Mns
50 µm
c
U#3
Trt
200 µm
d
Trt
Trt
200 µm
e
Man
Man
100 µm
f
Prp
Sps
Prp
100 µm
g
Prb
U#1
Mns
100 µm
h
Hsm
U#2
Mns
100 µm

ciation with hematite, magnetite contains significant amounts of Mn, Ni and Zn (4–5% MnO, 2–3% NiO and 0.1–0.6% ZnO).

Silicate layers

Spessartine in idiomorphic crystals is the main constituent of silicate-rich beds. One sample, Pigl.6,

TABLE 3. RESULTS OF ELECTRON-MICROPROBE ANALYSES OF SOME SILICATES FROM THE PIPJI Mn-RICH ROCKS

	Manganocummingtonite			Spessartine			Pennantite			Biotite			Rib?
Number	24			14			8			8			4
Sample	Pigl. 6			Pigl. 6			Pigl. 5			Pigl. 6			Pigl.5
	Ave.	Min.	Max.	Ave.	Min.	Max.	Ave.	Min.	Max.	Ave.	Min.	Max.	Ave.
V_2O_5 wt%		<0.04	0.07	0.08	<0.04	0.17	<0.05		0.05	<0.03		0.05	0.04
As_2O_5	<0.05					0.05	<0.05		<0.05	<0.05		<0.05	<0.04
SiO_2	56.28	53.06	57.61	33.78	32.35	34.94	18.81	18.51	19.07	41.92	39.97	44.91	24.49
Al_2O_3	0.18	0.05	0.29	18.01	18.01	18.01	27.48	26.92	28.04	9.03	6.55	10.21	<0.04
TiO_2		<0.05	0.05	0.19	0.07	0.30				0.07	0.03	0.11	
MgO	20.35	18.37	21.24	0.21	0.13	0.27	7.79	6.66	9.11	22.38	21.72	23.52	2.49
FeO	5.14	3.23	9.71	5.36	3.92	6.62	<0.05		<0.05	6.18	5.89	6.76	0.04
MnO	13.94	12.24	16.08	34.86	32.24	36.52	26.59	24.63	28.70	1.41	1.19	1.65	67.93
NiO	0.22	0.06	0.43			0.05	2.08	1.86	2.27	0.81	0.47	1.38	0.04
CoO	0.03	<0.05	0.08			≤0.07	1.42	1.35	1.47	<0.03		0.06	0.04
CaO	1.80	0.73	2.60	4.18	2.99	6.68	<0.04	<0.04	0.07	0.22	0.14	0.36	0.11
Na_2O	0.20	0.05	0.50			<0.04	0.03	<0.03	0.05	<0.04		0.07	<0.04
SrO	<0.05					<0.04	<0.04		<0.04	<0.04		<0.04	<0.04
BaO	0.02	<0.05	0.10			0.07	0.02		0.05	<0.04		0.07	≤0.17
PbO	0.05	<0.05	0.21	0.05	<0.04	0.13	<0.03		0.10	0.29	<0.05	0.87	≤0.10
K_2O						<0.04				7.69	4.45	9.17	
F	<0.08					0.11				4.45	3.32	5.16	
H_2O	2.11	2.01	2.14				10.58			2.31	2.06	2.70	3.69
-(O-F)										1.87	1.40	2.17	
Total	100.35	96.57	101.98	96.72	94.26	98.81	94.80	93.72	96.14	94.89	92.76	96.72	98.87
V *apfu*	<0.01	<0.01	0.01	<0.01		0.01	<0.01		<0.01	<0.01		<0.01	<0.01
As							<0.01		<0.01	<0.01		<0.01	<0.01
Si	8.00	7.86	8.12	2.87	2.79	2.94	2.13	2.10	2.17	2.84	2.72	3.15	1.99
Ti	<0.01			0.01		0.02				<0.01		0.01	
^{IV}Al				0.12	0.21	0.04	1.87	1.82	1.90				
Sum	8.01	7.86	8.12	3.00			4.00	4.00	4.00	2.84	2.72	3.16	1.99
^{VI}Al	0.03	0.01	0.05	1.68			1.80	1.77	1.84	0.72	0.54	0.80	<0.01
Mg	4.31	4.02	4.46	0.03	0.02	0.03	1.32	1.13	1.54	2.26	2.19	2.34	0.30
Fe	0.61	0.38	1.21	0.38	0.28	0.46	<0.01		<0.01	0.35	0.33	0.28	<0.01
Mn	1.68	1.53	1.94	2.51	2.34	2.62	2.55	2.36	2.76	0.08	0.07	0.09	4.68
Ni	0.03	0.01	0.05				0.19	0.17	0.20	0.04	0.03	0.08	<0.01
Co	0.00	0.00	0.01				0.13	0.12	0.13	<0.01	<0.01	<0.01	<0.01
Ca	0.27	0.12	0.39	0.38	0.27	0.61	<0.01		0.01	0.02	0.01	0.03	0.01
Na	0.06	0.01	0.13			≤0.01	0.01		<0.01	<0.01		0.01	<0.01
K	0.00	0.00	0.01				<0.01		<0.01	0.67	0.40	0.78	
Sr	0.00	0.00	0.01				<0.01		<0.01			<0.01	<0.01
Ba	<0.01						<0.01		<0.01	<0.01		<0.01	≤0.01
Pb	<0.01						<0.01		<0.01	0.01		0.02	<0.01
Sum	6.99			4.98			6.00			4.15	3.84	4.30	4.99
H	2.00						8.00	8.00	8.00	1.05	0.92	1.26	2.00
F										0.95	0.74	1.08	
O	23.99	23.86	24.12				17.95	17.95	17.95	9.92	9.65	10.49	9.99

Rib?: ribbeite ?

contains spessartine crystals that host numerous tiny inclusions of fluorapatite concentrated in the core of the porphyroblasts (Figs. 4f, 5a). Coarser-grained (10–30 μm) fluorapatite occurs in the main schistosity. The fluorapatite inclusions measure less than 5 μm and commonly display a subhedral to euhedral habit (Fig. 5b). The lattice parameter *a* of the spessartine calculated from the powder X-ray-diffraction data is 11.637(1) Å. EMP analyses of spessartine rims give the average composition $Sps_{80}Adr_{10}Alm_{10}$ (Table 3). The textural relationship between spessartine and fluorapatite is similar to that described from the carbonate-hosted syngenetic deposit of Bergwiesen in Val Ferrera, Swiss Alps (Brugger & Gieré 2000), but the fluorapatite at Pipji is very pure, containing less than 0.05 wt% As_2O_5 and SrO. Manganocummingtonite (Leake *et al*. 1997) occurs sporadically as prismatic to acicular crystals in silicates beds with porphyroblasts of spessartine; the chemical formula is $(Mg_{4.08}Mn_{1.58}Fe^{2+}_{1.02}Ca_{0.19})_{\Sigma 6.87}Si_{8.03}O_{22}(OH)_2$, with $0.76 \le Mg/(Mg + Fe^{2+}) \le 0.85$ (Table 3). The olivine-group mineral tephroite, Mn_2SiO_4, forms sporadic small xenomorphic aggregates with a near-end-member composition. Rare xenomorphic grains of chalcopyrite and idiomorphic crystals of pyrite occur in Pigl.6 with the spessartine porphyroblasts and manganocummingtonite. Pyrophanite occurs only as very small lamellae included in the rim of spessartine porphyroblasts. An average result of six EMP analyses leads to the following formula: $(Mn_{0.99}Fe_{0.03}Ca_{0.04})_{\Sigma 1.06}Ti_{0.93}O_{2.93}$ (Table 2). Rhodochrosite occurs rarely as large white-pink crystals with manganocummingtonite and spessartine.

Discordant veinlets

The Mn-rich horizons are cross-cut, commonly at high angle relative to S_0/S_1, by veinlets 1–3 mm wide composed mainly of white to pink rhodochrosite. Kutnohorite is rarer than rhodochrosite in this association, forming small equigranular grains. In Pigl.7, the center of the veinlet is occupied by manganite (γ-MnOOH) and crednerite. Crednerite, a rare Cu^+–Mn^{3+} oxide (Töpfer *et al*. 1995), forms needles up to 200 μm in length, completely enclosed in manganite and rhodochrosite (Fig. 4e). EMP analyses show that Mn^{3+} and Cu^+ are partially replaced by Ni, Co and Mg (up to 0.29 wt% NiO, up to 0.29 wt% CoO and 0.75 wt% MgO; Table 2). The chemical formula of crednerite is $Cu_{0.96}(Mn_{1.00}Mg_{0.03}Co_{0.005}Ni_{0.004})_{\Sigma 1.04}O_{2.02}$ (Table 2). Its unit-cell parameters are *a* 5.547(7), *b* 2.900(4), *c* 5.880(8) Å, β 103.84(5)°. Pennantite, ideally $(Mn,Al)_6(Si,Al)_4O_{10}(OH)_8$, appears as reddish brown lamellae up to 1 mm in length enclosed in carbonates (Table 3). The composition of this pennantite is similar to that associated with galaxite and alleghanyite in the Haute-Maurienne suite (Chopin 1978). Titanite occurs rarely as idiomorphic golden yellow crystals associated with pennantite.

Weathering

An alteration of probably Quaternary age resulted in the partial or complete oxidation of the minerals in the matrix and in the veinlets (Fig. 3). The most extreme alteration and oxidation of the primary Mn-rich assem-

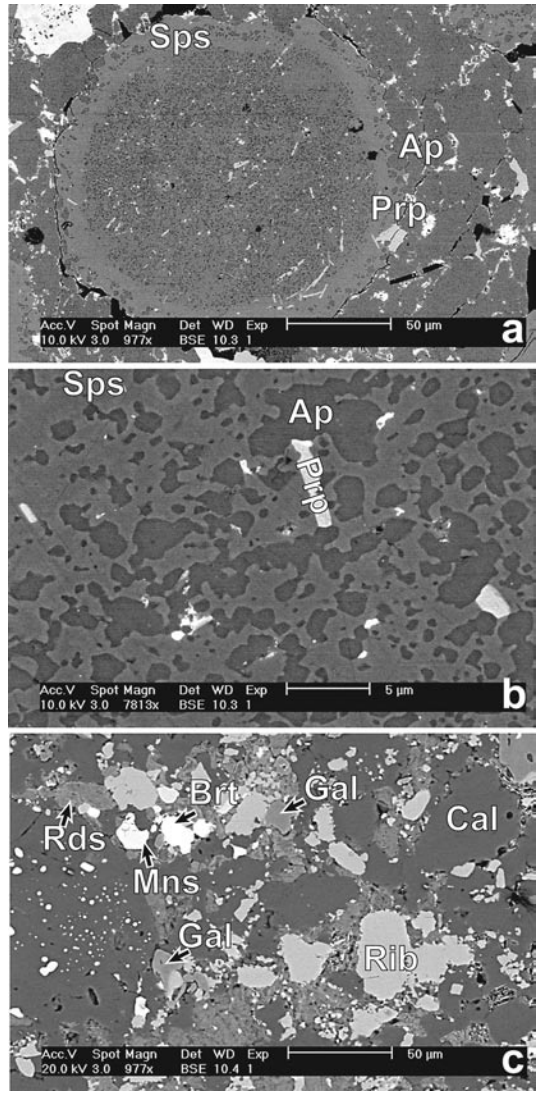

FIG. 5. Scanning electron microscope images of spessartine- and galaxite-bearing rocks from Pipji. (a) Spessartine porphyroblast with fluorapatite inclusions in coarser-grained apatite-bearing schist. Pigl.6, back-scattered-electron (BSE) image, 10 kV. (b) Detailed view of the central region of spessartine crystal in (a). Pigl.6, BSE, 10 kV. (c) Galaxite-bearing paragenesis. Pigl.5, BSE, 20 kV. The symbols are defined in Table 1.

blage result in black botryoidal concretions up to 10 cm in thickness. Pyrolusite, nsutite–ramsdellite, takanarite, cupriferous todorokite and hollandite are present in the oxidized assemblage.

Mineralogy of the Vanadates and Arsenates

Vanadium minerals occur mainly in the jacobsite- and manganosite-bearing rocks (Table 1). Results of chemical analyses of the various minerals are provided in Table 4. The most widespread vanadates are pyrobelonite and reppiaite. The pyrobelonite, ideally $PbMn^{2+}(VO_4)(OH)$, may contain significant quantities of Sr (up to 5.44 wt% SrO) and Ba (up to 1.56 wt% BaO), which account for up to ~20 mol.% of the Pb site. Reppiaite, ideally $Mn^{2+}{}_5(OH)_4(VO_4)_2$, is a rare mineral previously reported only from the type locality in Val Graveglia, Italy (Basso *et al.* 1992), and its presence

TABLE 4. RESULTS OF ELECTRON-MICROPROBE ANALYSES OF VANADATES FROM THE PIPJI Mn-RICH ROCKS

Mineral	Unknown #1			Unknown #2				Unknown#3			Turtmannite			Pyrobelonite			Sarkinite			Reppiaite		
No. of pts	19			14			2	6			14			18			8			13		
Sample	Pigl. 3n (XRD684,693)			Pigl. 3n			Pigl. 2b	Pigl. 2b						Pigl. 3n, 5			Pigl. 2b, 3n, 5			Pigl. 2b, 3n, 5		
	ave.	min.	max.	ave.	min.	max.		ave.	min.	max.	ave.	min.	max.	ave.	min.	max.	ave.	min.	max.	ave.	min.	max.
V_2O_5 wt%	18.75	17.93	19.75	12.12	11.42	12.80	9.51	9.65	6.47	10.81	7.42	6.51	8.75	23.71	23.12	25.11	3.06	2.51	4.88	21.50	16.13	26.88
As_2O_5	5.75	4.94	6.91	2.31	1.62	2.77	6.56	7.16	5.84	8.83	8.42	6.96	9.64	0.01	b.d.l.	0.07	37.98	35.23	40.46	12.26	5.45	18.19
SiO_2	0.06	b.d.l.	0.21	5.47	5.24	5.63	5.64	5.91	5.37	7.74	8.62	8.25	9.65	0.03	b.d.l.	0.22	0.07	<0.04	0.20	0.05	b.d.l.	0.18
CaO	0.12	0.10	0.16	0.10	0.01	0.18	0.11	0.68	0.05	3.15	0.13	0.05	0.23	0.46	0.27	0.97	0.46	0.41	0.56	0.10	0.02	0.29
MgO	1.58	1.17	2.53	3.09	1.78	4.24	5.86	7.18	6.74	7.73	6.63	5.96	8.09	0.13	b.d.l.	0.72	0.33	0.08	0.67	2.63	0.87	3.29
MnO	60.27	58.23	61.57	62.33	60.90	63.86	58.47	54.64	52.44	56.27	55.62	53.01	56.88	16.96	16.17	19.24	54.05	53.06	55.34	56.51	54.29	58.04
FeO	b.d.l.	b.d.l.	b.d.l.	b.d.l.	b.d.l.	b.d.l.	b.d.l.	b.d.l.	b.d.l.	b.d.l.	b.d.l.	b.d.l.	b.d.l.	b.d.l.	b.d.l.	b.d.l.	<0.04			0.01	b.d.l.	0.03
PbO	0.02	b.d.l.	0.10	0.02	b.d.l.	0.12	0.04	0.04	b.d.l.	0.14	0.01	b.d.l.	0.07	51.33	42.69	53.92	0.06	<0.05	0.16	0.02	b.d.l.	0.07
SrO	0.08	b.d.l.	0.16	0.01	b.d.l.	0.07	b.d.l.	b.d.l.	b.d.l.	b.d.l.	b.d.l.	b.d.l.	b.d.l.	1.33	0.63	5.44	<0.05			0.07	b.d.l.	0.09
BaO	0.02	b.d.l.	0.06	0.01	b.d.l.	0.07	0.05	0.05	b.d.l.	0.10	0.06	b.d.l.	0.25	0.40	0.06	1.56	<0.07			0.02	b.d.l.	0.07
Al_2O_3	0.02	b.d.l.	0.03	0.45	0.34	0.55	0.56	0.51	0.44	0.60	0.66	0.51	0.79	b.d.l.	b.d.l.	0.02	<0.04			0.01	b.d.l.	0.01
CoO	0.04	b.d.l.	0.11	0.08	0.03	0.16	0.12	0.05	0.02	0.08	0.05	b.d.l.	0.13	0.10	0.03	0.19	<0.04			0.04	0.03	0.06
NiO	0.07	b.d.l.	0.14	0.28	0.14	0.44	0.38	0.35	0.23	0.43	0.26	0.18	0.38	0.19	b.d.l.	0.38	<0.04			0.12	0.09	0.14
Cu_2O	0.01	b.d.l.	0.05	b.d.l.	b.d.l.	0.04	b.d.l.	0.01	b.d.l.	0.06	0.02	b.d.l.	0.08	0.02	b.d.l.	0.11				0.02	b.d.l.	0.07
ZnO	0.03	b.d.l.	0.10	0.06	b.d.l.	0.14	0.05	0.07	0.03	0.18	0.09	b.d.l.	0.23	0.03	b.d.l.	0.14				0.05	0.03	0.07
Na_2O	0.01	b.d.l.	0.04	0.01	b.d.l.	0.04	b.d.l.	0.01	b.d.l.	0.02	0.02	b.d.l.	0.06	0.02	b.d.l.	0.10	<0.05			0.01	b.d.l.	0.02
H_2O	13.83	13.68	14.02	13.88	13.62	14.08	14.22	8.81	8.73	8.88	8.13	7.99	8.27	4.58	4.48	4.92	3.44	3.40	3.50	6.24	5.86	6.45
Sum	100.66	99.84	101.51	100.21	98.88	101.15	101.57	95.12	94.20	96.17	96.13	94.80	97.63	99.30	98.18	100.16	99.45	98.65	101.81	99.64	96.34	102.54
V	1.61	1.53	1.70	3.29	3.09	3.43	2.52	2.39	1.60	2.66	1.90	1.69	2.25	1.03	1.00	1.04	0.09	0.07	0.14	1.37	1.09	1.69
As^{5+}	0.39	0.33	0.47	0.50	0.35	0.60	1.37	1.40	1.14	1.74	0.70	0.38	0.96	b.d.l.	b.d.l.	b.d.l.	0.87	0.80	0.91	0.62	0.27	0.97
As^{3+}											1.00	1.00	1.00						0.01			
Si	0.01	b.d.l.	0.03	2.25	2.13	2.34	2.26	2.21	2.03	2.89	3.34	3.21	3.67	b.d.l.	b.d.l.	0.01	<0.01	<0.01	0.01	b.d.l.	b.d.l.	0.02
Sum	2.01	1.93	2.08	6.03	5.77	6.23	6.15	6.00	5.86	6.21	6.94	6.87	7.13	1.03	1.00	1.04	0.96	0.94	0.99	1.99	1.89	2.06
Mg	0.31	0.23	0.48	1.89	1.10	2.59	3.50	4.01	3.76	4.35	3.83	3.50	4.66	0.01	b.d.l.	0.07	0.02	<0.01	0.04	0.38	0.13	0.47
Ca	0.02	0.01	0.02	0.04	0.01	0.08	0.05	0.27	0.02	1.26	0.05	0.02	0.10	0.03	0.02	0.06	0.02	0.02	0.03	0.01	b.d.l.	0.03
Mn	6.64	6.43	6.77	21.67	20.97	22.35	19.85	17.33	16.60	17.78	18.23	17.36	18.66	0.94	0.91	0.99	2.00	1.97	2.02	4.60	4.51	4.80
Fe	b.d.l.	b.d.l.	b.d.l.	b.d.l.	b.d.l.	b.d.l.	b.d.l.	b.d.l.	b.d.l.	b.d.l.	b.d.l.	b.d.l.	b.d.l.	b.d.l.	b.d.l.	b.d.l.				b.d.l.	b.d.l.	b.d.l.
Pb	b.d.l.	b.d.l.	b.d.l.	b.d.l.	b.d.l.	0.01	b.d.l.	b.d.l.	b.d.l.	0.01	b.d.l.	b.d.l.	0.01	0.90	0.70	0.97	<0.01	<0.01	<0.01	b.d.l.	b.d.l.	b.d.l.
Sr	0.01	b.d.l.	0.01	b.d.l.	b.d.l.	0.02	b.d.l.	b.d.l.	b.d.l.	b.d.l.	b.d.l.	b.d.l.	b.d.l.	0.05	0.02	0.19				b.d.l.	b.d.l.	0.01
Ba	b.d.l.	b.d.l.	b.d.l.	b.d.l.	b.d.l.	0.01	0.01	0.01	b.d.l.	0.01	0.01	b.d.l.	0.04	0.01	b.d.l.	0.04				b.d.l.	b.d.l.	b.d.l.
Al	b.d.l.	b.d.l.	0.01	0.22	0.17	0.26	0.26	0.22	0.19	0.27	0.30	0.23	0.36	b.d.l.	b.d.l.	b.d.l.				b.d.l.	b.d.l.	b.d.l.
Co	b.d.l.	b.d.l.	0.01	0.03	0.01	0.05	0.04	0.01	0.01	0.02	0.01	b.d.l.	0.04	0.01	b.d.l.	0.01				b.d.l.	b.d.l.	b.d.l.
Ni	0.01	b.d.l.	0.01	0.09	0.05	0.14	0.12	0.11	0.07	0.13	0.08	0.06	0.12	0.01	b.d.l.	0.02				0.01	b.d.l.	0.01
Cu	b.d.l.	b.d.l.	0.01	b.d.l.	b.d.l.	0.02	b.d.l.	b.d.l.	b.d.l.	0.02	0.01	b.d.l.	0.03	b.d.l.	b.d.l.	0.01				b.d.l.	b.d.l.	0.01
Zn	b.d.l.	b.d.l.	0.01	0.02	b.d.l.	0.04	0.01	0.02	0.01	0.05	0.03	b.d.l.	0.07	b.d.l.	b.d.l.	0.01				b.d.l.	b.d.l.	0.01
Na	b.d.l.	b.d.l.	0.01	0.01	b.d.l.	0.03	b.d.l.	0.01	b.d.l.	0.02	0.01	b.d.l.	0.05	b.d.l.	b.d.l.	0.01				b.d.l.	b.d.l.	b.d.l.
Sum	6.99	6.92	7.07	23.97	23.77	24.23	23.85	22.00	21.79	22.14	22.56	22.37	22.63	1.97	1.96	2.00	2.04	2.01	2.07	5.01	4.94	5.11
O	18.01	17.89	18.10	57.02	56.66	57.29	57.22	47.01	46.64	47.34	47.88	47.77	48.05	5.54	5.51	5.56	4.93	4.91	4.98	11.98	11.84	12.09
H	12.00	12.00	12.00	38.00	38.00	38.00	38.00	22.00			21.00	21.00	21.00	2.00	2.00	2.00	1.00	1.00	1.00	4.00	4.00	4.00

Normalization scheme: unknown #1: 9 cations per formula unit (*cpfu*), unknown #2: 30 *cpfu*, unknown #3: 28 *cpfu*, turtmannite: 29.50 *cpfu*, pyrobelonite: 3 *cpfu*, reppiaite: 7 *cpfu*. Simplified formula of unknown#1: $(V,As)_2(Mn,Mg)_7O_{18}H_{12}$, that of unknown #2: $(V,As,Si)_2SiMn_{12}O_{15}H_{20}$, and that of unknown #3: $(V,As,Si)(Mn,Mg)_4O_{9.5}H_6$. Appearance: unknown #1: orange xenomorphic grains in manganosite; unknown #2: orange needles in hausmannite; unknown #3: micaceous, dark orange phase; turtmannite: micaceous, yellow to light orange grains; pyrobelonite: red to dark red xenorphic grains, and reppiaite: dark orange grains. b.d.l.: below detection limit.

at Pipji has been confirmed by X-ray diffraction. The main difference in chemical composition between the Pipjigletscher and Val Graveglia occurrences resides in a more extended range in V:As ratio at Pipjigletscher, where V/(As + V) can be as low as 0.53 (average 0.69), compared to an average of 0.83 for the type locality (Basso *et al*. 1992; Fig. 6).

Turtmannite (Brugger *et al*. 2001) is a member of the hematolite–synadelphite group of minerals, closely related to mcgovernite and an unnamed phase from the Mn ores at the Kombat mine, Namibia (Dunn *et al*. 1988). Turtmannite is relatively common in the carbonate-rich layers of sample Pigl.2, where it occurs both in the S_1 schistosity and in discordant veinlets. Some of the veinlets appear to have crystallized under conditions similar to those during which the turtmannite became aligned in the main schistosity; the veinlet in Figure 4d cross-cuts a crystal of turtmannite, but new turtmannite crystallized during the opening of the vein, connecting the two fragments across the fracture. Brugger *et al*. (2001) recognized three variants of turtmannite in terms of site occupancy; the chemical formula of each variant is listed in Table 5. Each of these variants is characterized by a different ratio of high- and low-valence cations in the unit cell, $R_{H/L}$ = (As + V + Si) / (Mg + Mg + Al + Fe + Ca + Zn). In turtmannite, $R_{H/L}$ indicates the predominance of variant II (Fig. 6), although variant I dominates in the crystal used for the structure analysis.

In Pigl.2, the yellow to light orange turtmannite is associated with a dark orange mineral of very similar habit (Unknown #3; Fig. 4c) and related composition (Table 4). Compared to turtmannite, Unknown #3 has a low Si/(As + V + Si) value and a lower $R_{H/L}$. Another chemically related mineral, Unknown #2, has been recognized in the two manganosite-bearing samples, where it occurs sparsely as small orange needles in hausmannite (Figs. 4a, h). Unknown #2 has a Si/(As + V + Si) value similar to that of Unknown #3, but a smaller $R_{H/L}$. In the absence of X-ray data, we assume that unknown phases #2 and #3 are probably related to the mcgovernite group, and to turtmannite in particular.

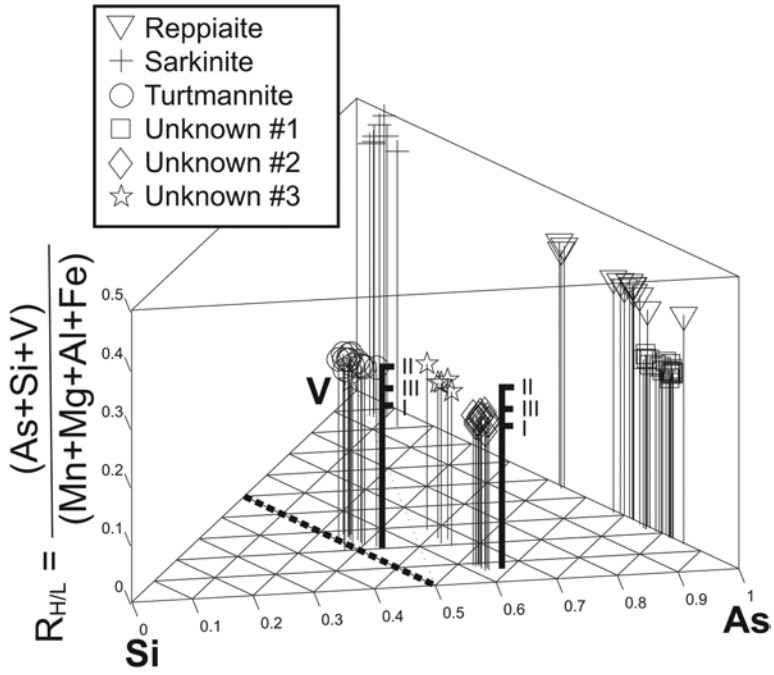

FIG. 6. Three-dimensional plot illustrating the chemical differences among the various Mn–Mg–V–As–Si minerals from Pipjigletscher. The basis triangle shows the atom ratios involving Si, V, and As. The bold dashed line shows the theoretical composition of turtmannite (Brugger *et al*. 2001), assuming no mixing between the Si and (V, As) sites. The ratio of the tetrahedrally coordinated high-valence cations (As + Si + V), including potential pyramidal As^{3+}, to the remaining cations is plotted along the vertical axis; this ratio is characteristic of the site-occupancy variants in mcgovernite-type minerals (Brugger *et al*. 2001). The heights corresponding to the three different site-occupancy variants recognized in turtmannite are plotted (I, II, III).

The $R_{H/L}$ value indicates a predominance of the arsenite-free variant III in Unknown #2 and #3, as opposed to turtmannite, where the arsenite-bearing site-occupancy variant II usually appears to dominate (Table 4). Unknown #2 also contains a significant amount of site-occupancy variant I.

Another unknown vanadate has been recognized on the basis of EMPA results. Unknown #1 is a very pure manganese vanadate, with a chemical composition identical to that of the arsenate allactite, $Mn_7(AsO_4)_2(OH)_8$. It forms orange xenomorphic grains up to 40 μm in diameter in Pigl.3n (Fig. 4g), where it is associated with pyrobelonite, reppiaite and Unknown #2 (Table 1).

Apart from the Mn-rich rocks from Pipji, another vanadium enrichment in the sediments of the Barrhorn Series is documented by the occurrence of vanadium-bearing muscovite (Al:V ≈ 4:1) in a block of white marble of probable Malm age. The block was found in the lateral tillite of the Brunegglетscher in Turtmanntal. This emerald-green muscovite forms platy crystals up to 2 mm and is enriched in stratiform beds up to 1 cm in thickness. It is associated with minor amounts of tetrahedrite, altered to powdery vésigniéite, $Cu_3Ba(VO_4)_2(OH)_2$.

Whole-Rock Geochemistry

Ten samples representing different mineralogical compositions were analyzed for major and trace elements at the Service d'Analyse des Roches du CNRS, Nancy, France by ICP–AES (Jobin–Yvon JY 70), ICP–MS (Perkin Elmer 5000), ion-specific electrode (F; fusion with sodium tetraborate followed by separation) and atomic absorption (Li; Perkin Elmer 5000). Samples for ICP and atomic absorption were dissolved by fusion with lithium tetraborate followed by acid dissolution. The mineralogical composition of these ten samples was analyzed qualitatively by X-ray diffraction (Philips PW 1771). Results on the 10 samples are presented in Table 6. In this section, we

TABLE 5. VALUES OF THE (V + As + Si)/(Mn + Fe + Al + Mg) RATIO (R) FOR SOME MINERALS* FROM PIPJIGLETSCHER

Mineral	$R_{H/L}$	σ_{n-1}
Unknown #1	0.289	0.007
Unknown #2	0.254	0.008
Unknown #3	0.279	0.009
Turtmannite	0.310	0.004

Occ. Var.	$R_{H/L}$	Formula
I	0.235	$^{[V]}(Mn,Mg)_{21}[(V,As)O_4]_3[SiO_4]_3O_3(OH)_{20}$
II	0.312	$^{[IV]}Mn_{1.5}{}^{[VI]}(Mn,Mg)_{21}[(V,As)O_4]_3[SiO_4]_3[AsO_3](OH)_{21}$
III	0.267	$^{[IV]}Mn_{1.5}{}^{[VI]}(Mn,Mg)_{21}[(V,As)O_4]_3[SiO_4]_2[SiO_3OH](OH)_{25}$

* including the three occupational variants (Occ. Var.) determined in the crystal-structure investigation of turtmannite by Brugger *et al.* (2001).

TABLE 6. PROPORTION OF MAJOR MINERALS AND BULK COMPOSITION OF THE Mn–Fe-RICH ROCKS FROM PIPJI

	Pigl. 4	Pigl. 6	Pigl. 7	Pigl. 9	Pigl. 50	Pigl. 51	Pigl. 52	Pigl. 53	Pigl. 54	Pigl. 55
Jacobsite	×××		×××		×		×××	××	×××	××
Kutnohorite	××		×××			×	×××	××	××	×××
Rhodochrosite	×××	×××	××		×××	×××	××	×××	×××	××
Spessartine		×××	o	×		×				×?
Magnetite				×		××				
Hematite		×?		×××						
Fluorapatite		×								
Barite	×		×		o		o?	o	××	×
Mangano-cummingtonite		××		×	××	×		×		
Clinochlore (pennantite)		×	××		×				××	×
Talc-2*M*	××									
Paragonite	×						×			
SiO_2 wt%	6.92	14.4	3.86	2.51	13.1	4.84	3.54	10.4	6.92	3.11
Al_2O_3	1.06	5.86	1.30	1.11	2.64	2.03	0.87	3.59	1.87	0.64
Fe_2O_3	9.58	6.84	24.9	78.5	10.9	12.0	22.3	13.4	22.7	11.11
MnO	52.3	32.2	38.6	5.28	40.1	43.7	41.2	39.7	45.0	47.36
MgO	0.97	3.54	2.41	0.42	5.29	3.32	1.50	3.84	1.90	1.60
CaO	7.91	15.7	10.7	3.78	6.16	7.66	13.0	8.39	5.07	11.9
TiO_2	<0.05	0.22	<0.05	<0.05	0.09	<0.05	<0.05	0.06	<0.05	<0.05
P_2O_5	0.70	5.19	0.55	0.46	1.84	1.07	0.35	1.49	0.37	0.43
LOI	18.5	14.0	17.6	3.17	18.6	25.6	17.5	19.8	15.9	20.9
F	0.14	0.66	0.17	0.05	0.29	0.13	0.06	0.18	0.13	0.07
Total	98.1	98.5	100.0	95.3	99.0	100.3	100.2	100.8	99.8	97.1
As ppm	1111	297	257	44	541	89	179	659	247	128
Ba	19355	2564	11299	14773	20378	1481	11137	3961	13381	22770
Cd	1.59	0.73	0.53	bdl	bdl	0.30	0.60	bdl	0.67	1.30
Ce	6.31	17.63	4.06	2.30	8.51	5.27	3.18	6.78	4.54	2.87
Co	866	706	486	487	580	433	538	567	438	567
Cr	12	39	16	11	31	15	12	33	14	<10
Cs	<0.2	0.84	<0.2	0.23	0.21	0.36	<0.2	0.31	0.48	<0.2
Cu	149	128	21	144	6	121	241	34	17	345
Dy	0.43	3.37	0.32	0.36	1.00	0.78	0.31	0.98	0.41	0.32
Er	0.20	2.31	0.15	0.19	0.63	0.55	0.16	0.60	0.23	0.14
Eu	n/a	0.60	n/a	n/a	n/a	n/a	n/a	0.35	n/a	n/a
Ga	16	14	14	6	15	16	13	17	18	15
Gd	0.33	3.28	0.39	0.34	1.24	0.73	0.33	1.09	0.46	0.34
Ge	4.20	2.99	2.46	2.49	3.17	2.15	2.72	3.11	5.37	4.73
Hf	0.42	1.36	0.17	0.05	0.58	0.25	0.15	0.47	0.35	0.10
Ho	0.08	0.81	0.05	0.05	0.21	0.18	0.06	0.22	0.07	0.04
La	3.45	22.00	2.72	1.86	8.15	7.48	2.64	6.43	3.00	3.04
Lu	0.03	0.37	0.02	0.03	0.09	0.09	0.02	0.10	0.03	0.02
Mo	13.62	1.77	3.58	3.05	1.02	0.76	5.47	0.75	5.71	6.88
Nb	0.77	4.26	0.64	1.35	2.98	0.94	0.43	2.19	0.85	0.27
Nd	2.64	14.00	2.10	1.26	5.94	3.18	1.83	4.66	2.30	1.76
Ni	1801	901	996	753	1871	997	867	1779	1970	1424
Pb	17.5	12.5	38.0	18.3	3.5	6.4	60.7	5.0	8.5	32.0
Pr	0.70	3.45	0.58	0.31	1.50	0.83	0.47	1.13	0.53	0.48
Sb	11.9	0.5	37.9	6.0	4.5	0.5	15.5	1.5	19.9	14.2
Sm	0.55	2.78	0.40	0.27	1.04	0.60	0.35	0.98	0.43	0.32
Sn	1.47	3.07	<0.5	0.67	1.45	1.25	<0.5	0.81	0.63	<0.5
Sr	1900	421	965	95	1063	155	1768	270	877	3787
Ta	0.08	0.39	0.06	0.06	0.22	0.07	<0.01	0.15	0.08	<0.01
Tb	0.06	0.47	0.06	0.05	0.17	0.11	0.05	0.15	0.06	0.05
Th	1.32	4.55	0.83	0.63	1.41	0.94	0.29	1.50	1.12	0.20
Tm	0.033	0.35	0.022	0.032	0.10	0.087	0.023	0.097	0.031	0.023
U	6.57	3.43	3.94	5.05	2.55	4.60	4.70	3.39	9.96	3.99
V	988	164	504	1634	463	209	497	629	586	398
W	4.01	1.63	6.59	2.03	5.48	0.92	2.40	1.83	6.71	3.09
Y	2.55	52.73	1.72	3.76	12.25	11.19	1.74	12.82	2.57	1.59
Yb	0.22	2.28	0.14	0.19	0.60	0.54	0.17	0.64	0.20	0.12
Zn	850	282	658	257	583	321	504	512	830	485
Zr	16	53	11	8.7	28	12	10	25	19	11
Li	1.00	4.00	1.00	1.00	2.00	1.00	1.00	1.00	2.00	1.00
Cl	27	<20	54	<20	39	20	21	111	44	20
(La/Lu)cn	11.94	6.21	12.68	6.45	9.75	8.54	12.18	6.82	10.36	20.87
Ce/Ce*	0.96	0.48	0.77	0.71	0.58	0.50	0.68	0.60	0.86	0.56
Fe/(Fe+Mn)	0.14	0.16	0.36	0.93	0.19	0.20	0.32	0.23	0.31	0.17

Abundances of the minerals are estimated visually from the X-ray powder pattern. ×××: major phase (>30 vol.%), ××: abundant phase (>10 vol.%), × present (>5 vol.%), o: near limit of detection (1–5 wt%). The following elements were monitored but found to be below the detection limit (bdl) in all ten samples: Na_2O <0.05%, K_2O <0.05%, Be: <1.5 ppm. n/a: not analyzed.

summarize the main results and compare the composition of the Mn- and Fe-rich rocks at Pipji to that of other Alpine occurrences of various genesis listed in Table 7, including hydrogenous seawater oolitic Fe-ores formed from seawater with no hydrothermal input, residual freshwater Fe ores of the siderolitic, syngenetic exhalative radiolarite-hosted (oceanic) Mn–Fe ores, and syngenetic exhalative carbonate-hosted Mn–Fe ores (Gonzen, Val Ferrera).

The Mn-rich rocks from Pipji show a relatively small range in Fe/(Fe + Mn) molar ratios, with values between 0.14 and 0.32 (Fig. 7). Only one Fe-rich sample was analyzed (Pigl.9), characterized by a high Fe/(Fe + Mn) value of 0.93. The small range in Fe/(Fe + Mn) values of the Mn-rich sediments is similar to the results from the Radiolarite-hosted exhalative ores, but contrasts with the Val Ferrera suite, which is characterized by the abundance of mixed Fe–Mn silicate–oxide

TABLE 7. LOCATION, GENETIC TYPE AND METAMORPHISM GRADES OF THE OCCURRENCES OF Fe- AND Mn-RICH SEDIMENTS AND METASEDIMENTS MENTIONED IN THE TEXT

Type and Localities	Genesis	Metamorphism	Anal.	Reference
Oolitic Fe-deposits				
In the Alps: Chamoson, VS [1]; Erzegg, BE [2]; Scharmandlager; Glärnisch, SG [3]; Windgälle, BE [4]	Syngenetic without relation to hydrothermal event (hydrogenous)	Diagenesis to lower greenschist facies	XRF	Serneels, unpubl. data
In the Jura: Herznach, AG [5]	*idem*	Diagenesis	XRF	Serneels, unpubl. data
Siderolitic Fe-deposits				
In the Jura: Salève, GE [6]; Ferreyres, VD [7]; Montcherrand, VD [8]; Lajoux, Souboz, and Boecourt, JU [9]; Mervellier and Liesberg, BE [10]; Lausen, BL [11]; Otelfingen, ZH [12]; Klettgau, SH [13]	Enrichments of mostly Fe-hydroxides within karst (residual)	Diagenesis	XRF	Serneels (1993)
In the Alps: Dents du Midi, VS [14]	*idem*	Anchizone	XRF	Serneels (1993)
Radiolarite-hosted Mn deposits				
Falotta and Parsettens, GR [15] and numerous other occurrences, *e.g.*, Fornogletscher, Gr [17]	Hydrothermal syngenetic deposit near an oceanic ridge	Zeolite (Falotta, Parsettens) to amphibolite (Forno) facies	XRF	Suana (1984)
Ködnitz Valley, Austria [16]	*idem*	Greenschist facies	-	Abrecht (1990)
Praborna, Aosta Valley, Italy [18]	*idem*	Eclogite facies	-	Martin-Vernizzi (1984)
Val Graveglia, Liguria, Italy [19]	*idem*	Zeolite to greenschist facies	-	Cortesogno *et al.* (1979)
Haute Maurienne, France [20]	*idem*	Blueschist facies	-	Chopin (1978)
Carbonate-hosted Fe-Mn deposits				
Gonzen Fe-Mn deposit, SG [22]	Hydrothermal syngenetic within-platform carbonates	Zeolite facies	XRF	Pfeifer *et al.* (1988)
Val Ferrera, GR [21]	*idem*	Greenschist to blueschist facies	XRF ICP-MS	Brugger & Gieré (2000)
Pipji, Turtmanntal, VS [23]	Hydrothermal syngenetic?	Upper green-schist facies	XRF ICP-MS	This paper
Fe- and Al-rich karst fillings				
Apuane Alps, Italy [24], Liguria, Italy [25], La Vanoise, France [26] and Prealps, Switzerland [27]	Residuals sediments in karstic cavities	Zeolite facies to greenschist facies	-	Poinssot *et al.* (1997)

The numbers in bracket refer to the map in Figure 1. For the localities included in the geochemical comparison with Pipji, the analytical techniques used for geochemical analysis are mentioned.

ores. A similar situation exists at Gonzen. The Mn–Fe lenses from Pipji are SiO_2-poor (<16 wt%), in contrast to Radiolarite and Val Ferrera ores (up to >80 wt% SiO_2; Fig. 8b). The Pipji rocks are also relatively Al-poor (Fig. 8a), and there is a good positive correlation between Al_2O_3 and TiO_2.

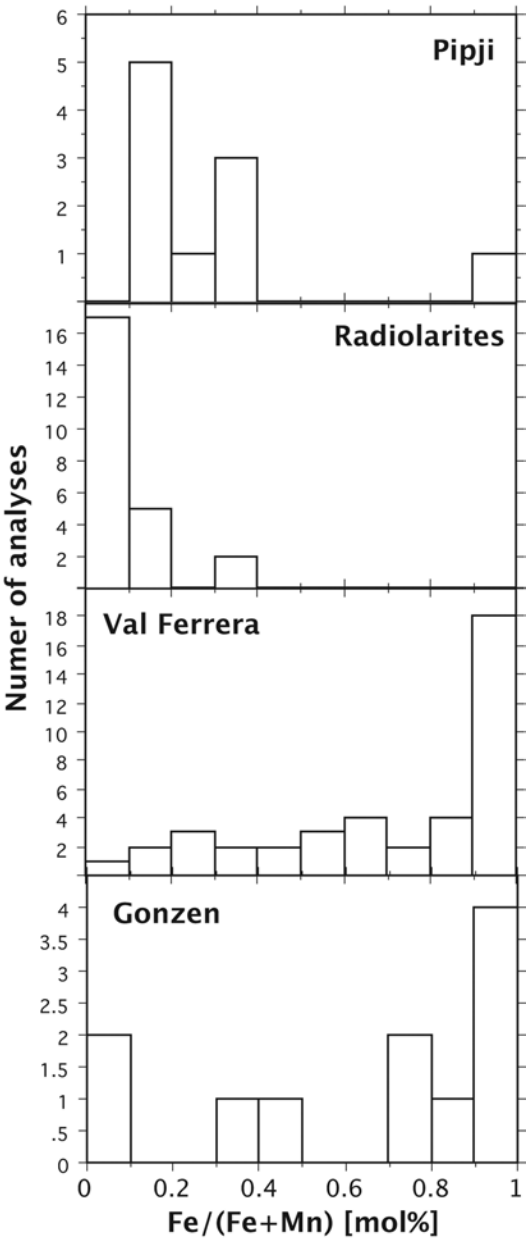

FIG. 7. Values of Fe/(Fe + Mn) (mole%) in Mn- and Fe-rich sediments from Pipji compared with those from other carbonate-hosted (Val Ferrera and Gonzen) and radiolarite-hosted deposits.

The Mn-rich rocks of Pipji contain relatively high levels of transition elements (*e.g.*, up to 1801 ppm Ni, 866 ppm Co and 850 ppm Zn). This contrasts with relatively low concentrations in the ores from Val Ferrera and radiolarite-hosted deposits (Fig. 8d, Table 7). The Pipji rocks have highly variable REE contents (Fig. 9). The samples with lowest REE contents also have the lowest Al contents, and display relatively flat REE pattern relative to Post-Archean Australian Shales (PAAS; McLennan 1989; Fig. 9). In contrast, the samples with highest REE contents show a strong enrichment in heavy REE (HREE) as well as a well-developed negative Ce anomaly relative to PAAS. These samples also have the highest Al contents. Three samples show an intermediate character (Fig. 9). The high variability and the low concentrations of REE at Pipji contrast with the REE patterns reported for two samples of "bauxite" from the Prealps and Vanoise (Fig. 9), but mimic closely the range of values obtained for the carbonate-hosted Fe–Mn ores of Val Ferrera (Fig. 9). Li and Be, elements typically enriched in the aluminous continental sediments of the Briançonnais Domain, are present only in very low concentrations at Pipji. Similarly, F concentration is elevated only in the one sample enriched in fluorapatite (Pigl.6; Table 6).

DISCUSSION

Geochemistry and genesis

We consider three possibilities for the formation of the Mn-rich lenses at Pipji: (1) Precipitation of colloidal Mn oxyhydroxides in karstic pockets at the interface between phreatic water and seawater during marine transgression (hydrogenous origin), (2) mixing of hydrothermal fluid with marine or freshwater, either in a karstic system during the Middle Jurassic or at the sediment–water interface in the Triassic. (3) Accumulation of reworked residual sediments in a freshwater system (residual origin). The Pipji Mn-rich rocks may represent an unusual, Mn-rich variety of Middle Jurassic continental sediments.

The fine compositional banding of many Pipji manganiferous rocks represents a pre-metamorphism feature, and is most consistent with a syngenetic origin of the Mn-rich rock, as a chemical precipitate (*e.g.*, Nicholson 1992). An early, syngenetic or diagenetic origin is also suggested by the alternation of Mn-rich layers with Triassic carbonates.

A number of geochemical discrimination diagrams have been developed to distinguish among hydrothermal, hydrogenous and residual Mn-rich rocks; these are based upon both major and trace elements. Poinssot *et al.* (1997) demonstrated that little mobility of trace elements occurred in Alpine Al-rich sediments during metamorphism, except for a depletion in low-field-

strength elements (Rb, Ba, Sr), and slight enrichments in some transition metals (Co, Ni, Zn), actinides (U), and REE (Ce). We therefore assume that the chemical composition of the Pipji ores probably reflects closely the original, pre-metamorphism state.

Toth (1980) developed a diagram based upon the Al and Si contents of the ores, later modified by Crerar *et al*. (1982), to distinguish among hydrothermal, hydrogenous-detrital and detrital-diagenetic deposits (Fig. 8b). The diagram relies on the contrasting behavior of Si and Al in hydrothermal fluids and during weathering. Silicon is soluble in hydrothermal fluids and is efficiently precipitated upon cooling, whereas Al is only poorly soluble. In hydrothermal deposits, most Al comes with the detrital input. During weathering, Al is enriched in the residual sediments, whereas Si is depleted. The Al–Si diagram discriminates accurately most ores, but fails in the case of Si-poor carbonate-hosted exhalative ores that contain a large portion of Mn carbonates (*e.g*., Gonzen; Nsuta, Mucke *et al*. 1999). This failure may reflect either undersaturation of the hydrothermal fluid with respect to SiO_2 or very low-temperature hydrothermal fluids (<<100°C). The Pipji ores are Al- and Si-poor; they overlap the Gonzen ores in the detrital-hydrogenous field; in both deposits, both Si and Al probably have a detrital origin, in agreement with their position in the Si–Al diagram. This common detrital origin of Al and Si is further supported by the positive correlation between Si and Al concentrations; indeed, the samples from Pipji plot along the field boundary between "hydrogenous-detrital" and "detrital-diagenetic", overlapping the detrital-residual oolitic ores of Jura and Alps (Fig. 4b). The detrital origin of Al is also clearly supported by a good correlation between Al and the poorly soluble elements Zr and Ti.

High Na and Mg contents have been linked to a genesis as chemical sediments from seawater (Nicholson 1992). The Mg contents of the Pipji ores suggest a marine origin, but they contrast with very low Na contents. This feature may indicate leaching of Na during greenschist-facies metamorphism; on the other hand, the Mg content may be related to influx from

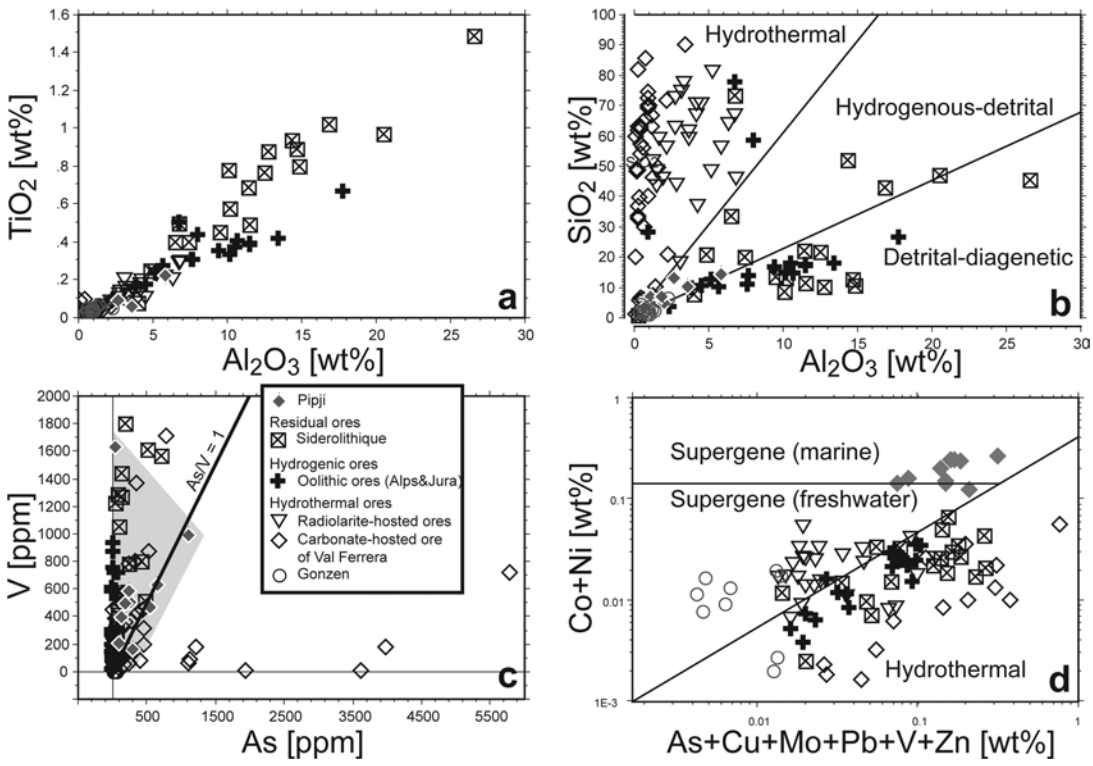

FIG. 8. Geochemical variation diagrams used in deciphering the origin of the Pipji Mn- and Fe-rich lenses, and comparison with the composition of other Alpine Fe and Mn deposits (see Table 7). (a) TiO_2 *versus* Al_2O_3 diagram, showing the good correlation between these two elements, resulting from their input as detrital components; (b) SiO_2 *versus* Al_2O_3 diagram from Toth (1980) and Crerar *et al*. (1982); (c) V *versus* As diagram; (d) diagram of Nicholson (1992) to discriminate between hydrothermal and supergene deposits.

the dolomitic host-rock, and not to interaction with seawater. Hence, the Na:Mg ratio does not seem to be useful to decipher the origin of the Pipji ores.

The proportion of trace elements in Mn- or Fe-rich syngenetic hydrothermal, hydrogenous or residual sediments is controlled mainly by sorption, as Mn and Fe exist as poorly crystalline oxides and oxyhydroxides exhibiting large surface-area and surface-charge (*e.g.*, Point of Zero Charge of 3.2 for todorokite, 2.8 for birnessite, 7.2 for pyrolusite; Yopps & Fuerstenau 1964). Bonatti *et al.* (1972) proposed to use concentrations of transition elements (Co + Ni + Cu) to discriminate between modern deep-sea hydrothermal and hydrogenous deposits, the latter being progressively more enriched in transition elements. This observation results from the kinetics of trace-metal incorporation in Mn oxyhydroxides. Hydrothermal deposits form relatively quickly (hours to years), whereas deep-sea polymetallic nodules grow slowly (>1000 years) under condition of low input of detritus, and hence have plenty of time to scavenge transition metals from seawater by sorption. Therefore, the diagram by Bonatti *et al.* (1972) is not well suited for discrimination of hydrothermal and hydrogenous ores in a non-oceanic context, and in particular in carbonate-hosted and continental deposits, because of higher rates of sedimentation. Nicholson (1992) proposed a generally applicable diagram based on the concentration and proportion of transition metals (Fig. 4d). Applied to Alpine ores, this diagram shows equivocal results. The Val Ferrera ores plot correctly inside the hydrothermal field, but most of the hydrothermal radiolarite-hosted ores plot in the freshwater supergene field. Siderolitic and oolitic ores plot next to the hydrothermal-supergene boundary, but most of them are located in the hydrothermal field. The Pipji Mn-rich rocks occupy a distinct position in this diagram, in the supergene (marine) field.

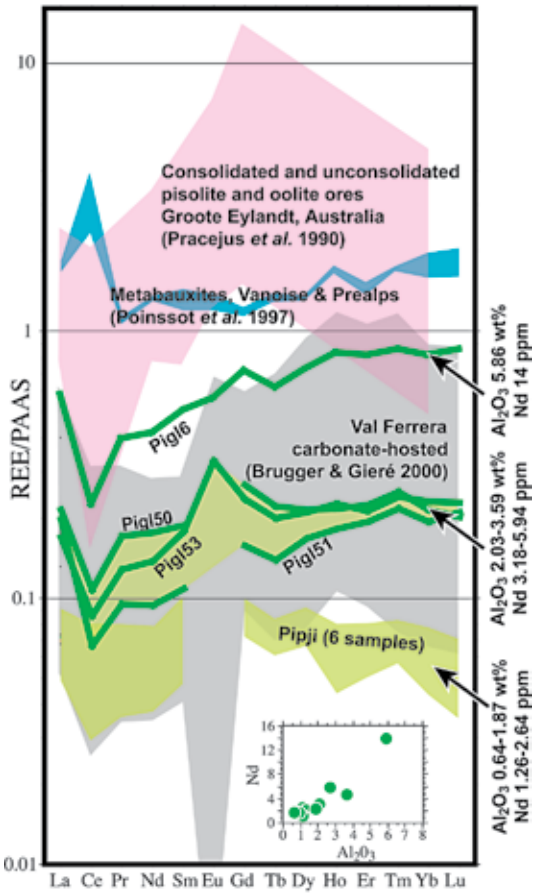

FIG. 9. Comparison of REE patterns of Pipji Mn–Fe-rich rocks with those of some other Mn and Fe ores. The REE patterns are normalized with the Post-Archean Australian Shales (PAAS, McLennan 1989).

Arsenic and V are elements that are both easily absorbed on oxyhydroxides of Fe and Mn (*e.g.*, Bowell 1994), and hence it comes as no surprise that they are enriched in all types of Fe- and Mn-rich sediments (Fig. 4c). In general, high V contents are associated with a hydrogenous origin, whereas a high As:V ratio indicates a proximal hydrothermal input (Brugger & Gieré 2000). The Val Ferrera ores show two independent trends, one As-rich and one V-rich. In contrast, the siderolitic and oolitic ores show low As:V values. The Pipji Mn-rich rocks have generally low As:V values, but three samples plot along the As = V line (Fig. 4c). The low As:V values and high concentrations of V could be genetically related to the occurrence of vanadium-bearing muscovite in the Malm of the Barrhorn Series: in the former case, V is scavenged from seawater on Fe–Mn oxyhydroxides, in the latter case by clay minerals.

Bonatti *et al.* (1972) proposed to use the U:Th ratio to distinguish between hydrothermal and hydrogenous deposits. Hydrogenous deposits are considered enriched in Th relative to hydrothermal deposits owing to their slow rate of accumulation and longer exposure to seawater. The Pipji Mn-rich rocks have low Th contents (most have < 2 ppm Th), and plot in the hydrothermal field defined by Bonatti *et al.* (1972).

The REE have been shown to be an excellent indicator of the origin of modern deep-sea Fe and Mn mineralization (*e.g.*, Mills & Elderfield 1995). In the Pipji Mn-rich rocks, the shape of the REE pattern and the concentration of the REE are correlated with the Al contents. As the Al content of the Fe–Mn lenses is related to a detrital input (micas and clays), this correlation indicates that the REE in the Al-rich samples also have a probable detrital origin. This detrital component is characterized by a negative Ce anomaly and the heavy rare-earth elements (HREE) enrichment relative to PAAS (Fig. 9). The detrital component hence appears to

be different from that in the unequivocal metabauxites from Vanoise and Prealps, which display a positive Ce anomaly and only a very slight HREE enrichment (Fig. 9). The REE signature of the detrital component at Pipji bears some similarity with the REE signature of the hydrogenous Mn-ores of Groote Eylandt and their reworked equivalent, in terms of negative Ce-anomaly and general enrichment in HREE (Fig. 9).

In contrast to those samples from Pipji showing a relatively large detrital component, the five samples with the lowest concentrations of REE and hence lowest detrital input of REE plot in a relatively narrow range, and represent another end-member composition for the REE components in the Fe–Mn-rich rocks. This second component is characterized by very low REE contents (< 0.1 times PAAS), a negative or no anomaly in Ce, and a slight enrichment in medium REE relative to PAAS. This component is very similar to the end-member hydrothermal component in the carbonate-hosted Mn–Fe ores of Val Ferrera (Brugger & Gieré 2000). Hence, we interpret this second component as representing a hydrothermal input of the REE.

The REE hence appear to provide the strongest evidence for a hydrothermal origin of the Pipji Mn–Fe-rich rocks. This origin is also supported by the low U and Th contents and by the range in As:V values. The low Si contents strongly suggest a low temperature (≤60°C) for the mineralizing solutions; as the Pipji Mn-rich lenses are located next to the basement, we consider it unlikely that highly quartz-unsaturated fluids would occur in this geological environment.

Assemblage of metamorphic minerals

The complex mineral assemblage observed today developed during the Tertiary Alpine metamorphism. One characteristic of the Pipjigletscher occurrence, in contrast with other Alpine deposits of Mn [*e.g.*, Fianel: Brugger & Gieré (1999); Falotta and Parsettens: Geiger (1948); Liguria: Cortesogno *et al.* (1979)], is the presence of a reduced paragenesis including native copper and manganosite, and the abundance of mixed-valence phases containing As^{3+} and As^{5+} (turtmannite), Fe^{2+} and Fe^{3+} (magnetite) and Mn^{2+} and Mn^{3+} (hausmannite). Manganosite occurs in relatively large quantities in the Fe–Mn ores hosted by Upper Jurassic carbonates (Helvetic domain) at Gonzen (Epprecht 1946, Pfeifer *et al.* 1988). There, manganosite developed during the very low-grade Alpine metamorphism along veins. In the Briançonnais domain, Poinssot *et al.* (1997) noted the increase of the Fe^{2+}:Fe^{3+} ratio between unmetamorphosed and metamorphosed aluminous sediments. The relatively reduced paragenesis in the Mn-rich lenses at Pipjigletscher thus probably results from the interaction between metamorphic fluids containing both CO_2 and CH_4 through equilibration with the organic-matter-rich host rocks (dark dolomitic marble) and the manganiferous lenses, whose protolith had probably high Mn^{4+}:Mn^{2+} values (Fig. 10).

Oxides and carbonates of Fe and Mn carry the bulk of the Fe and Mn in the pockets, whereas silicates (spessartine and tephroite) are abundant only locally. Jacobsite is the most characteristic ore-mineral. In the Mn–Fe–CO_2–H_2O–$O_{2(g)}$ compositional space, jacobsite coexists with rhodochrosite, magnetite, hausmannite or manganosite. The relations among these associations have been investigated using $O_{2(g)}$ *versus* pH diagrams (Fig. 10). The sources of the thermodynamic properties are given in the figure caption. The absence of large-scale evidence for Fe or Mn mobility within the lenses during metamorphism indicates a low fluid:rock ratio during metamorphism. In the carbonate-poor diagram, a temperature change from 450 to 350°C does not significantly affect the topology of the diagram, in both the Mn-rich (Figs. 10a, b) and Fe-rich (Figs. 10e, f) subspaces. In the Mn-rich subspace, jacobsite can coexist with manganosite and hausmannite, the two oxides of Mn found at Pipjigletscher in close association in the S_1 schistosity. The assemblage jacobsite + hausmannite + manganosite occurs at a log $f(O_{2(g)})$ of –20.3, one log unit above the magnetite–hematite buffer at –21.6 (450°C, 4 kbar). However, for higher partial pressures of $CO_{2(g)}$ (2.5%), a large field with jacobsite + rhodochrosite appears between the jacobsite + manganosite and jacobsite + hausmannite fields at 450°C, shifting the field for coexisting jacobsite and manganosite to oxygen fugacities well below the magnetite–hematite buffer (Fig. 10c).

At lower temperature, the stability field of rhodochrosite increases markedly at the expense of jacobsite (Fig. 10). Rhodochrosite is a very minor phase in the groundmass of the Pipjigletscher Mn-rich rocks, in contrast to kutnohorite, which is a very abundant S_0–S_1 carbonate. This indicates a higher stability of kutnohorite relative to rhodochrosite in the relatively Ca-rich rocks at Pipjigletscher.

Besides kutnohorite, the major Mn phases not accounted for in the system Mn–Fe–CO_2–H_2O–O_2 are tephroite, spessartine, and galaxite. Tephroite is a common silicate in Mn-rich rocks under amphibolite-facies and higher-grade conditions, but has also been described in some deposits metamorphosed under conditions of the lower- to upper-greenschist facies (*e.g.*, Innes & Chaplin 1986, Ashley 1989, Brugger & Gieré 2000, respectively). The local abundance of spessartine and, locally, galaxite, reflects the local abundance of Al. Galaxite occurs in silica-undersaturated, Mn- and Al-rich rocks (Essene & Peacor 1983) subjected to metamorphism ranging from the lower greenschist facies (*e.g.*, Kombat mine, Namibia; Innes & Chaplin 1986) to the granulite facies (*e.g.*, Gnos & Peters 1995). The galaxite from Pipjigletscher shows a large component of spinel (Table 2), but only very limited solid-solution with jacobsite and hausmannite, two spinel-group minerals found in the same hand-specimen.

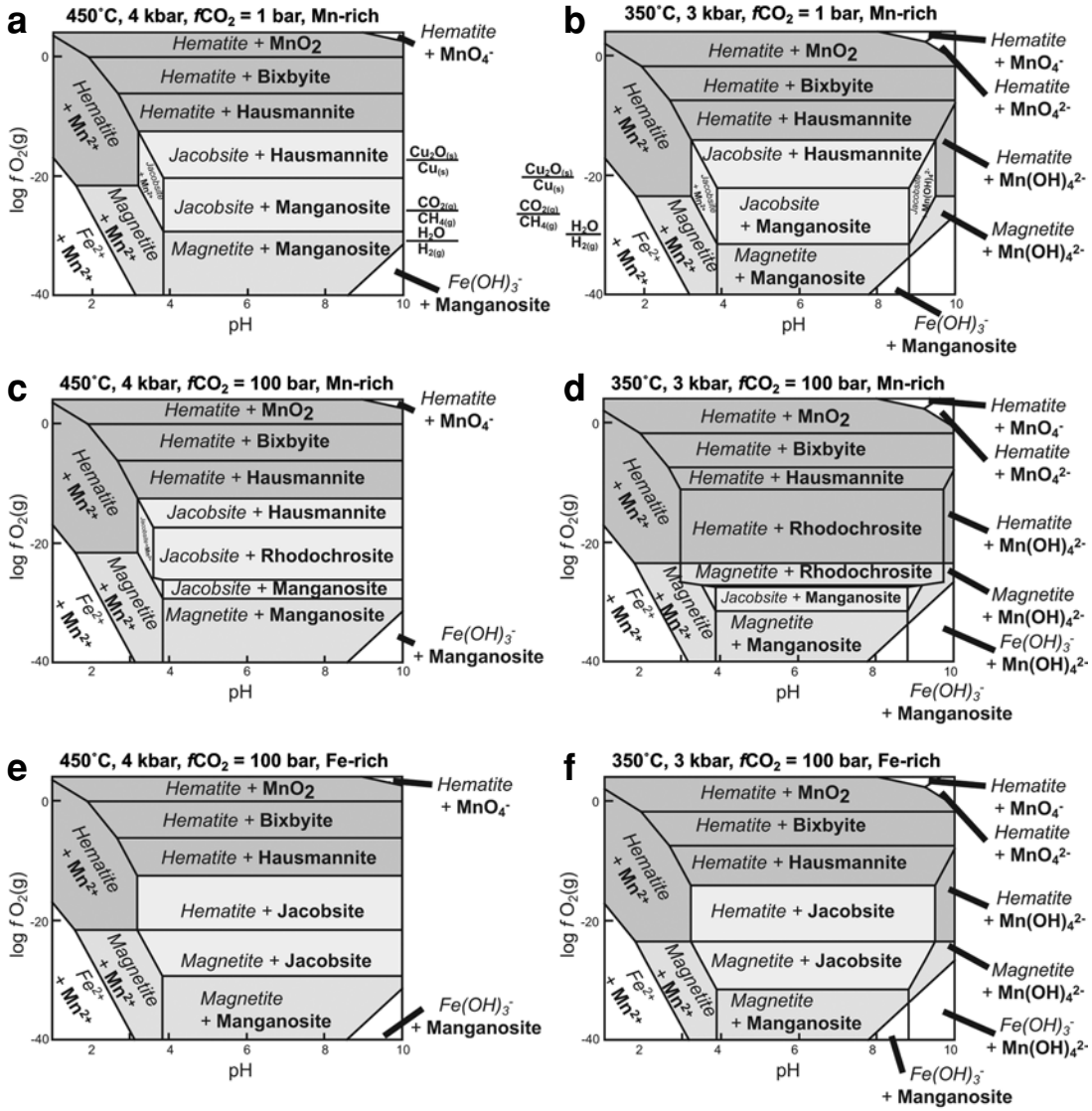

FIG. 10. Log $a(O_{2(g)})$ *versus* pH diagram for the Fe–Mn–CO_2–H_2O–O_2 system at 450°C, 4 kbar and 350°C, 3 kbar. Thermodynamic properties are extrapolated to high pressures and temperatures using SUPCRT92 (Johnson *et al.* 1992). Standard thermodynamic properties for aqueous species, gases and Fe-bearing minerals are taken from the SUPCRT database; for manganese minerals, they are from Robie *et al.* (1995), and for jacobsite, from Binnewies & Milke (1999). The diagrams are drawn for two different chemical subsystems: $0 \le Fe:Mn \le 2$ (Mn-rich part; a to d), and $0 \le Mn:Fe \le 0.5$ (Fe-rich part; e, f). The diagrams are plotted using the THERMOCHEMISTRY package (Turnbull & Wadsley 1977).

DISCUSSION AND CONCLUSIONS

The pre-metamorphic mineral assemblage at Pipji most likely consisted of highly oxidized (Fe^{3+}, Mn^{4+}) chemical sediments deposited from low-temperature (<60°C) hydrothermal fluids upon mixing with seawater or fresh water. The primary mineral assemblage (Fe and Mn oxyhydroxides) favored the fixation, by sorption, of elements like As and V (*e.g.*, Brugger & Gieré 2000). The geochemistry of the Pipji Mn–Fe-rich rocks shows no relationship to the Middle Jurassic continental aluminous and ferruginous sediments of the Briançonnais

Domain; in particular, they are lacking enrichment in Be, Li, high-field-strength elements and REE characteristic of these deposits. The age of Mn precipitation at Pipji depends upon the interpretation of their geological setting. If they represent a paleokarst filling, a Middle Jurassic (Dogger) age is probable, whereas a Triassic syngenetic exhalative origin similar to the Val Ferrera deposits is likely otherwise. Owing to the geochemical similarity of the Mn-rich sediments at Pipji with the Val Ferrera Mn–Fe ores, and given the textural evidence for early, syngenetic or diagenetic enrichement in Mn, a Triassic syngenetic origin in most likely. Hence, the Pipji Mn–Fe-rich rocks are related to a number of similar deposits in the Piedmond, Briançonnais, and Helvetic domains of the Alps. All these deposits formed as a result of extensional tectonics, which favors the circulation of low-temperature hydrothermal fluid and its release into oxygenated surface or near-surface water.

The REE seem to be the most robust elements to discriminate between hydrothermal and hydrogenous – residual – diagenetic Fe–Mn ores. Although discrimination diagrams based upon transition metals are useful indicators within a particular depositional environment, their use cannot be generalized to the problem of deciphering the origin of Fe–Mn ores in dissimilar environments.

The complex mineralogical assemblage found in the manganiferous rocks at Pipjigletscher developed during greenschist-facies regional metamorphism. The redox conditions during metamorphism were at or below the hematite–magnetite buffer, whose position is close to that of the manganosite + hausmannite + jacobsite assemblage at 450°C, 4 kbar (Fig. 10). This reduced paragenesis developed under the influence of fluids buffered by the carbonate-"graphite" assemblage found in the dolomitic marble that hosts the Mn-rich lenses.

Acknowledgements

This work would not have been possible without the enthusiasm of M. Sartori, who brought his discovery of unusual rocks to the attention of one of us (N.M.), and who subsequently supported our study with his geological knowledge. We thank E.-A. Perseil for preliminary EMP analyses of some minerals, Vincent Serneels for kindly providing unpublished geochemical data for some Swiss Fe-ores, and Stefan Ansermet for help with field and photographic work. We are grateful to Philippe Thélin (XRD laboratory, Institute of Mineralogy and Geochemistry, UNIL, Lausanne) for XRD-microanalysis facilities, and Peter O. Baumgartner (SEM laboratory, Institute of Geology and Paleontology, UNIL, Lausanne) for the help with the SEM–EDS. The paper benefitted from thorough reviews by Jens Gutzmer, Walter E. Trzcienski Jr. and Robert F. Martin.

References

Abrecht, J. (1990): An As-rich manganiferous mineral assemblage from the Ködnitz Valley (Eastern Alps, Austria): geology, mineralogy, genetic considerations, and implications for metamorphic Mn. *Neues Jahrb. Mineral., Monatsh.*, 363-375.

Ashley, P.M. (1989): Geochemistry and mineralogy of tephroite-bearing rocks from the Hoskins manganese mine, New South Wales, Australia. *Neues Jahrb. Mineral., Abh.* **161**, 85-111.

Basso, R., Lucchetti, G., Zefiro, L. & Palenzona, A. (1992): Reppiaite, $Mn_5(OH)_4(VO_4)_2$, a new mineral from Val Graveglia (northern Apennines, Italy). *Z. Kristallogr.* **201**, 223-234.

Baud, A., Masson, H. & Septfontaine, M. (1977): Karst et paléotectonique Jurassiques du domaine Briançonnais des Préalpes. *In* Symposium Sédimentation Jurassique Ouest-Européenne (Paris). *A.G.F. Publ. Spéc.* **1**, 441-450.

Berthelsen, A., Burollet, P., Dal Piaz, G.V., Franke, W. & Trümpy, R. (1992): Tectonics. *In* Atlas of Compiled Data – a Continent Revealed – the European Geotraverse (R.M. Freeman, ed.). Cambridge University Press, Cambridge, U.K. (3-5).

Binnewies, M. & Milke, E. (1999): *Thermochemical Data of Elements and Compounds*. John Wiley & Sons Ltd, New York, N.Y.

Bonatti, E., Kramer, T. & Rydell, H. (1972): Classification and genesis of sub-marine iron manganese deposits. *In* Ferromanganese Deposits on the Ocean Floor (D. Horn, ed.). National Science Foundation, Washington, D.C. (146-165).

Bowell, R.J. (1994): Sorption of arsenic by iron oxides and oxyhydroxides in soils. *Appl. Geochem.* **9**, 279-286.

Brugger, J., Armbruster, T., Meisser, N., Hejny, C. & Grobety, B. (2001): Description and crystal structure of turtmannite, a new mineral with a 68 Å period related to mcgovernite. *Am. Mineral.* **86**, 1494-1505.

Brugger, J. & Gieré, R. (1999): As, Sb, and Ce enrichment in minerals from a metamorphosed Fe–Mn deposit (Val Ferrera, Eastern Swiss Alps). *Can. Mineral.* **37**, 37-52.

Brugger, J. & Gieré, R. (2000): Origin and distribution of some trace elements in metamorphosed Fe–Mn deposits, Val Ferrera, Eastern Swiss Alps. *Can. Mineral.* **38**, 1075-1101.

Chopin, C. (1978): Les paragenèses réduites ou oxydées des concentrations manganésifères des "schistes lustrés" de Haute-Maurienne (Alpes françaises). *Bull. Minéral.* **101**, 514-531.

Chopin, C., Goffé, B., Ungaretti, L. & Oberti, R. (2003): Magnesiostaurolite and zincostaurolite; mineral description with a petrogenetic and crystal-chemical update. *Eur. J. Mineral.* **15**, 167-176.

Cortesogno, L., Lucchetti, G. & Penco, A.M. (1979): Le mineralizzazioni a manganese nei diaspri delle ofioliti liguri: mineralogia e genesi. *Rend. Soc. Ital. Mineral. Petrol.* **35**, 151-197.

CRERAR, D.A., NAMSON, J., CHYI, M., WILLIAMS, L. & PENCO, A.M. (1982): Manganiferous cherts of the Franciscan assemblage. I. General geology, ancient and modern analogues, and implications for hydrothermal convection at oceanic spreading centers. *Econ. Geol.* **77**, 519-540.

DUNN, P.J., FRANCIS, C.A. & INNES, J. (1988): A mcgovernite-like mineral and leucophoenicite from the Kombat mine, Namibia. *Am. Mineral.* **73**, 1182-1185.

EPPRECHT, W. (1946): Die Eisen- und Manganerze der Gonzen. *Beiträge zur Geologie der Schweiz, Geotechnische Serie* **24**.

ESCHER, A., MASSON, H. & STECK, A. (1987): Coupes géologiques des Alpes occidentales suisses. *Service Hydrologique et géologique national , Rapports géologiques* **2**.

ESSENE, E.J. & PEACOR, D.R. (1983): Crystal chemistry and petrology of coexisting galaxite and jacobsite and other spinel solutions and solvi. *Am. Mineral.* **68**, 449-455.

GEIGER, T. (1948): Manganerz in den Radiolariten Graubündens. *Beiträge zur Geologie der Schweiz, Geotechnische Serie* **27**.

GNOS, E. & PETERS, T. (1995): Tephroite–hausmannite–galaxite from a granulite-facies manganese rock of the United Arab Emirates. *Contrib. Mineral. Petrol.* **120**, 372-377.

INNES, J. & CHAPLIN, R.C. (1986): Ore bodies of the Kombat mine, South West Africa – Namibia. In Mineral Deposits of Southern Africa (C.R. Anhaesser & S. Maske, eds.). Geol. Soc. South Africa, Johannesburg, Republic of South Africa, 1789-1805.

JOHNSON, J.W., OELKERS, E.H. & HELGESON, H.C. (1992): SUPCRT92: a software package for calculating the standard molal thermodynamic properties of minerals, gases, aqueous species and reactions from 1 to 5000 bars and 0° to 1000°C. *Comput. Geosci.* **18**, 899-920.

LEAKE, B.E., WOOLLEY, A.R., ARPS, C.E.S., BIRCH, W.D., GILBERT, M.C., GRICE, J.D., HAWTHORNE, F.C., KATO, A., KISCH, H.J., KRIVOVICHEV, V.G., LINTHOUT, K., LAIRD, J., MANDARINO, J.A., MARESCH, W.V., NICKEL, E.H., ROCK, N.M.S., SCHUMACHER, J.C., SMITH, D.C., STEPHENSON, N.C.N., UNGARETTI, L., WHITTAKER, E.J.W. & GUO, YOUZHI (1997): Nomenclature of amphiboles: report of the subcommittee on amphiboles of the International Mineralogical Association, Commission on New Minerals and Mineral Names. *Can. Mineral.* **35**, 219-246.

MARTIN-VERNIZZI, S. (1984): *La mine de Praborna (Val d'Aoste, Italie): une série manganésifère métamorphisée dans le faciès éclogite*. Thèse de doctorat, Université Pierre et Marie Curie, Paris, France.

MCLENNAN, S.M. (1989): Rare earth elements in sedimentary rocks: influence of provenance and sedimentary processes *In* Geochemistry and Mineralogy of Rare Earth Elements (B.R. Lipin & G.A. McKay, eds.). *Rev. Mineral.* **21**, 169-200.

MEISSER, N., ANSERMET, A., BRUGGER, J. & WÜLSER, P.A. (2004) : Alpine metamorphised ore deposits: gardens of rare or new minerals for mineralogical museums. *Mineralogy & Museums, 5th Congress (Paris)*.

MILLS, R.A. & ELDERFIELD, H. (1995): Rare earth element geochemistry of hydrothermal deposits from the active TAG Mound, 26°N Mid-Atlantic Ridge. *Geochim. Cosmochim. Acta* **59**, 3511-3524.

MUCKE, A., DZIGBODI-ADJIMAH, K. & ANNOR, A. (1999): Mineralogy, petrography, geochemistry and genesis of the Paleoproterozoic Birimian manganese-formation of Nsuta/Ghana. *Mineral. Deposita* **34**, 297-311.

NICHOLSON, K. (1992): Contrasting mineralogical-geochemical signatures of manganese oxides: guides to metallogenesis. *Econ. Geol.* **87**, 1253-1264.

PERSEIL, E.-A. & SMITH, D.C. (1995): Sb-rich titanite in the manganese concentrations at St. Marcel – Praborna, Aosta Valley, Italy: petrography and crystal chemistry. *Mineral. Mag.* **59**, 717-734.

PFEIFER, H.-R., OBERHÄNSLI, H. & EPPRECHT, W. (1988): Geochemical evidences for a synsedimentary hydrothermal origin of Jurassic iron–manganese deposits at Gonzen (Sargans, Helvetic Alps, Switzerland). *Marine Geol.* **84**, 257-272.

POINSSOT, C., GOFFÉ, B. & TOULHOAT, P. (1997): Geochemistry of the Triassic–Jurassic Alpine continental deposits: origin and geodynamic implications. *Bull. Soc. Géol. Fr.* **168**, 287-300.

ROBIE, R.A., HUEBNER, J.S. & HEMINGWAY, B.S. (1995): Heat capacities and thermodynamic properties of braunite (Mn_7SiO_{12}) and rhodonite ($MnSiO_3$). *Am. Mineral.* **80**, 560-575.

SARTORI (1990): L'unité du Barrhorn. *Mémoire de Géologie, Univ. de Lausanne* **6**.

SERNEELS, V. (1993): Le Sidérolithique Suisse. *Minaria Helvetica* **13b**, 74-83.

SMITH, D.C. & PERSEIL, E.-A. (1997): Sb-rich rutile in the manganese concentrations at St. Marcel-Praborna, Aosta Valley, Italy: petrology and crystal-chemistry. *Mineral. Mag.* **61**, 655-669.

STAMPFLI, G. (1993): Le Briançonnais, terrain exotique dans les Alpes? *Eclogae Geol. Helv.* **86**, 1-45.

SUANA, M. (1984) Die Manganerzlagerstätten von Tinizong (Oberhalbstein, Graubünden). *Beiträge zur Geologie der Schweiz, Geotechnische Serie* **64**.

TÖPFER, J., TRARI, M., GRAVEREAU, P., CHAMINADE, J.P. & COUMERC, J.P. (1995): Crystal growth and reinvestigation of the crystal structure of crednerite, $CuMnO_2$. *Z. Kristallogr.* **210**, 184-187.

TOTH, J.R. (1980): Deposition of submarine crusts rich in manganese and iron. *Geol. Soc. Am., Bull.* **91**, 44-54.

TURNBULL, A. & WADSLEY, M. (1977): THERMOCHEMISTRY SYSTEM, Version 5.0/5.2 (computer package).

YOPPS, J. & FUERSTENAU, D.W. (1964): The zero point of charge of alpha-alumina. *J. Colloid Sci.* **19**, 61-71.

Received July 13, 2004, revised manuscript accepted September 7, 2005.